Renewable Energy 256 (2026) 123757

Contents lists available at ScienceDirect

Renewable Energy

journal homepage: www.elsevier.com/locate/renene

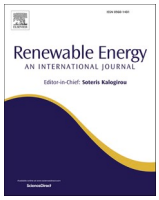

Multi-objective optimization, techno-economic analysis, and life cycle assessment of an innovative solar-biomass-driven cogeneration system integrated with MED-RO-MD: A case study of the Canary Islands

Seyed Alireza Mousavi Rabeti [a], Mohammad Hasan Khoshgoftar Manesh [a,*], Ana María Blanco-Marigorta [b,**], B. Del Río-Gamero [b]

[a] Energy, Environmental, and Biological Systems Research Lab (EEBRlab), Division of Thermal Sciences and Energy Systems, Department of Mechanical Engineering, Faculty of Technology & Engineering, University of Qom, Qom, Iran
[b] Department of Process Engineering, Universidad de Las Palmas de Gran Canaria, Las Palmas de Gran Canaria, Spain

ARTICLE INFO

Keywords:
Multi-objective optimization
Solar and biomass
Cogeneration
Life cycle assessment
Canary islands

ABSTRACT

Managing freshwater and electricity production in islands is vital for sustainability and reducing dependency on external resources, ensuring energy security and environmental protection. This study explores the design, analysis, and feasibility of an innovative biomass-solar cogeneration system that produces both power and freshwater for the Canary Islands, Spain. The proposed system design incorporates a combination of the Brayton cycle, steam Rankine cycle, and organic Rankine cycle for power generation, while integrating multi-effect distillation, reverse osmosis, and membrane distillation desalination for freshwater production. Additionally, a CO_2 capture unit is included to minimize environmental pollutant emissions. The solar field provides the necessary heat for the system via the solar tower, while the air-steam gasification unit supplies the required energy for the cycle using biomass. The biomass fuel selected is based on the local forest type, specifically Canary Pine Needles. Machine learning is applied to analyze the subsystems of the proposed system. The feasibility of the proposed system has been evaluated through technical-economic analysis and life cycle assessment. Dynamic modeling was performed based on the climatic conditions of Las Palmas. Finally, a sensitivity analysis and multi-objective optimization were conducted on the system's functional parameters. The objective functions in the optimization process included maximizing cogeneration efficiency, minimizing the payback period, and minimizing the total environmental impact rate. Three multi-objective optimization algorithms (NSGA-III, MOMVO, MOGOA) were used to optimize the proposed system. The results indicate that the proposed system achieves an average energy efficiency of 31.64 % and exergy efficiency of 14.35 % annually. The average levelized cost and environmental impact of electricity are calculated to be 0.19 $/kWh and 1.24 mPts/kWh, respectively. Additionally, the payback period for the system is estimated at 3.22 years. The multi-objective optimization of the proposed system resulted in a 54.04 % improvement in cogeneration efficiency, a 38.82 % reduction in payback period, and a 6.39 % decrease in the environmental impact rate, compared to the baseline performance of the system before optimization.

Nomenclature

A	Area (m^2)	*ORCP*	Organic Rankine Cycle Pump
AC	Air Compressor	*ORCT*	Organic Rankine Cycle Turbine
AD	Adsorption Desalination	*P*	Pressure (bar), Pump

(*continued on next column*)

(*continued*)

ANS	Annual Net Saving ($/year)	*PEC*	Purchase Equipment Cost ($)
AS	Annual Saving ($/year)	*PP*	Payback Period (Year)
b	Environmental Impact per Exergy (Pts/kJ)	*Q*	Heat (kW)
C	Carbon Composition	*RO*	Reverse Osmosis

(*continued on next page*)

This article is part of a special issue entitled: SI ECOS2024 published in Renewable Energy.

* Corresponding author.
** Corresponding author.
E-mail addresses: m.khoshgoftar@qom.ac.ir, mh.khoshgoftar@gmail.com (M.H. Khoshgoftar Manesh), Anamaria.blanco@ulpgc.es (A.M. Blanco-Marigorta).

https://doi.org/10.1016/j.renene.2025.123757
Received 6 January 2025; Received in revised form 5 April 2025; Accepted 11 June 2025
Available online 13 June 2025

(*continued*)

c	Cost per Exergy ($/kJ)	*ROP*	Reverse Osmosis Pump
CC	Combustion Chamber	r_p	Pressure ratio
CRF	Cost Recovery Factor	*RR*	Recovery ratio
D	Diameter (m)	*s*	Specific Entropy (kJ/kg.K)
DA	Deaerator	*SA*	Specific Area (m^2/kg)
DC	Direct Contact	*SHX*	Solar Heat Exchanger
DNI	Direct Normal Irradiation (W/m2)	*ST*	Steam Turbine
DV	Decision Variable	*Sup*	Superheater
Eco	Economizer	*T*	Temperature (K)
Eva	Evaporator	*TIP*	Turbine Inlet Pressure
Ex	Exergy (kW)	*TIT*	Turbine Inlet Temperature
FC	Fixed Cost ($)	*U*	Overall Heat Transfer Coefficient (W/m^2)
GAC	Gasification Air Compressor	*W*	Work (kW)
GP	Gasification Pump	*x*	Salinity (g/kg)
GT	Gas Turbine	*y*	Mole Fraction
h	Specific Enthalpy (kJ/kg)	*Y*	Environmental Impact Rate (Pts/s)
H	Hydrogen Composition	*Z*	Investment Cost Rate ($/s)
HDH	Humidification-Dehumidification	**Subscript**	
HRSG	Heat Recovery Steam Generator	*Bio*	Biomass
HRVG	Heat Recovery Vapor Generator	*G*	Gasification
HTF	Heat Transfer Fluid	*0*	Reference condition
i	Interest Rate	*B*	Brine
Ib_m	Environmental Impact per Weight (mPts/kg)	*ch*	chemical
J	Specific Mass Flow Rate (kg/s.m^2)	*cwd*	Cooling Water Discharge
LCA	Life Cycle Assessment	*D*	Distillate, Destruction
LHV	Lower Heating Value	*en*	End effect
m	Mass (kg)	*f*	Feed, Fuel
MC	Moisture Content	*k*	Component
MD	Membrane Distillation	*P*	Product
MED	Multi-effect Distillation	*ph*	Physical
MOGA	Multi-Objective Genetic Algorithms	*Q*	Heat
MOGOA	Multi-objective Grasshopper Optimization Algorithm	*s*	Steam
MOMVO	Multi-Objective Multi-Verse Optimization	*sw*	Seawater
MOPSO	Multi-Objective Particle Swarm Algorithms	*w*	Water, Work
MOWCA	Multi-Objective Water Cycle Algorithms	**Greek Symbols**	
N	Nitrogen Composition	η	Efficiency
n	Number of effect	μ	Dynamic Viscosity
N	Operation Working Hours	π	Osmosis Pressure
NPV	Net Present Value ($)	ρ	Density (kg/m^3)
NSGA-III	Non-dominated Sorting Genetic Algorithm III	ϕ	Maintenance Factor
O	Oxygen Composition	ψ	Exergy Efficiency
OF	Objective Function		
ORC	Organic Rankine Cycle		
ORCC	Organic Rankine Cycle Condenser		

1. Introduction

World population growth, global warming, and increasing demands for water and energy have placed significant pressure on resources worldwide [1]. Desalination systems, which have been effectively used on many islands and water-scarce regions, are a sustainable solution to reduce water stress worldwide [2]. The European Union (EU) has set strict policies to reduce emissions of environmental pollutants by more than half by 2030, making them mandatory for all member states [3]. Hybridizing renewable energy sources is a suitable solution to reduce uncertainty associated with renewable energy, enabling the production of cogeneration or polygeneration in energy systems [4]. Another technical option to reduce environmental pollutants, CO_2 capture is recognized as a highly effective solution. It is projected that the implementation of CO_2 capture technologies could contribute to a 14 % reduction in global CO_2 emissions by 2060 [5]. The importance of hybridizing renewable solar energy and biomass, employing CO_2 capture systems, employing hybrid desalination for sustainable production of freshwater, optimizing energy systems to reduce fuel consumption and costs, and integrating energy systems for simultaneous power and freshwater production has been discussed through a review of previous research.

The combination of solar energy and biomass is regarded as a sustainable solution for the development of energy systems. In this context, Khoshgoftar Manesh et al. [6] introduced an innovative solar-biomass-driven polygeneration system for energy supply in a tomato greenhouse. Three different types of biomass were investigated in their system, and a CO_2 capture unit was incorporated to reduce emissions. The results indicated that alfalfa is a suitable fuel in terms of both energy and environmental performance. The system achieved a net power generation of 215.30 kW, CO_2 removal of 2.68 tons/day, and freshwater production of 118.45 m^3/day. By combining solar energy and biomass in a polygeneration system for power, freshwater, and methanol production, the net power generation, freshwater production, and payback period were calculated as 62.86 MW, 63.88 kg/s, and 4.28 years, respectively [7]. Siddiqui and Dincer developed a novel solar energy-based rice husk gasification polygeneration system for producing hydrogen, freshwater, cooling, and electricity. The power generation achieved by the combined cycle is 12.9 MW, with a total energy efficiency of 46.8 % and an exergy efficiency of 47.8 % [8]. Khadimallah et al. [9] proposed a novel tri-generation system that integrates solar and biomass energy for the production of power, freshwater, and biogas. Their results indicate that with a solar field of 3.9 ha, the system can generate 34.55 MW of electricity and produce 783 m^3/h of freshwater. Bozgeyik et al. [10] conducted 4E analyses (energy, exergy, economic, and environmental) of a hybrid solar-biomass-geothermal polygeneration system, calculating power production at 7.76 MW and freshwater production at 6.16 kg/s. The energy and exergy efficiencies of the system were found to be 65.55 % and 27.09 %, respectively.

The use of CO_2 capture is a sustainable solution to mitigate the environmental impact of energy systems that rely on combustion processes for energy conversion. This approach helps in reducing greenhouse gas emissions, making energy production more environmentally friendly. In this regard, Khani et al. [11] utilized a CO_2 capture unit in a solar-fossil fuel-based polygeneration system to produce power, freshwater, and carbon dioxide for greenhouse applications. This integration not only reduced the system's carbon footprint but also enhanced its overall efficiency by providing multiple outputs, including a controlled supply of CO_2 for plant growth. Noorbakhsh et al. [12] investigated a novel fossil fuel-solar polygeneration system with integrated CO_2 capture for emissions reduction. Their results demonstrated that the system achieved an electricity cost of 142.94 $/MWh and an environmental impact of 330.77 Pts/MWh, highlighting the potential for both economic and environmental improvements through the inclusion of CO_2 capture technology. Zhu et al. [13] proposed an innovative biomass-fired Organic Rankine Cycle (ORC) integrated with CO_2 capture for the simultaneous production of power and heat. The results indicated that the biomass-fired ORC-CHP system, utilizing cyclopentane as the working fluid, demonstrated excellent thermodynamic performance, achieving the highest primary energy-saving ratio. This highlights the system's potential for improving both energy efficiency and sustainability in power and heat generation. In some applications, CO_2 capture is employed not only to mitigate environmental impacts but also to produce valuable by-products within energy systems. This dual benefit enhances the overall sustainability and economic viability of such systems, as captured CO_2 can be repurposed for industrial applications, such as enhanced oil recovery, the production of synthetic fuels, or chemical feedstocks, while simultaneously reducing greenhouse gas emissions. For instance, Khoshgoftar Manesh et al. [14] employed a CO_2 capture unit in a biomass-solar-wind polygeneration system to purify syngas produced through air-steam gasification for the production of valuable biofuel, specifically ammonia. This integration not only enhances the overall efficiency of biofuel production but also contributes

to reducing the environmental impact of the system by capturing and utilizing CO_2, thus offering a sustainable approach to energy generation and resource recovery. Ahmed investigated the conversion of coal to methanol and hydrogen as eco-friendly fuels by utilizing CO_2 capture technology. This approach aims to reduce the environmental impact of coal-based energy production, making it a more sustainable option by capturing and repurposing carbon dioxide emissions in the process [15].

Hybrid desalination systems offer a sustainable solution for freshwater production, enhancing output and enabling zero liquid discharge [16]. In this context, Chauhan et al. [17] introduced a solar-powered HDH-DCMD hybrid system, demonstrating nearly double the efficiency and freshwater output compared to standalone systems through detailed modeling and thermodynamic analysis. In another study, researchers developed a hybrid AD-DCMD system utilizing waste heat, achieving a 136.7 % increase in specific daily water production and reducing freshwater costs by up to 56.05 % compared to standalone AD systems [18]. Morid and Khoshgoftar Manesh [19] integrated a MEDAD system with power and cooling cycles, achieving significant gains, including a 95.25 % increase in freshwater production, 22 % fuel savings, a 5 % boost in power output, and 65.65 % overall efficiency. In another study, researchers integrated solar, wind, and hydrogen energy for a cogeneration system aimed at producing freshwater, power, and treating wastewater. The system combined microbial desalination cell, humidification-dehumidification, and reverse osmosis, achieving 720 kW of electricity and 5.36 m^3/h of freshwater with an energy efficiency of 22.09 % [20]. Hybrid desalination systems powered by renewable energy sources, such as solar and biomass, significantly enhance freshwater production efficiency, reduce fuel consumption, and lower environmental impacts, offering sustainable solutions to global water scarcity challenges.

Optimization in renewable cogeneration and polygeneration systems boosts efficiency, reduces costs, and minimizes environmental impact, ensuring sustainable and cost-effective performance [21]. In this regard, Mousavi Rabeti et al. [22] evaluated the integration of a solar-biomass polygeneration system with a hybrid solar-waste-fossil fuel cogeneration system. Their study found that municipal solid waste, as the most accessible fuel, provided favorable economic conditions, while the Salps swarm algorithm optimization improved system efficiency, reducing costs and environmental impact. Vazini Modabber and Khoshgoftar Manesh [23] optimized a trigeneration system on Qeshm Island using multi-objective genetic algorithms (MOGA) and multi-objective water cycle algorithms (MOWCA). The optimization, which included integrating MED with RO desalination and solar thermal collectors, increased exergetic efficiency by 12.66 %, reduced costs by 47.4$/h, and cut environmental impact by 49.2 pt/h. Mehrabian and Khoshgoftar Manesh [24] optimized a multi-generation system using seven algorithms, including multi-objective particle swarm optimization and Thompson sampling efficient multi-objective optimization. The optimization improved polygeneration efficiency to 51.84 % for municipal solid waste, reduced total cost rate to 0.181 US$/s, and decreased ecological impact rate to 128.50 Pt/h. The system's risk was also minimized, with municipal solid waste presenting lower risk than olive pits. In another study, the Qeshm plant's new configuration was optimized using the MOPSO algorithm. The optimization improved poly-generation efficiency by 5.523 %, net power output by 7.945 %, and reduced environmental impact by 3.98 %. It also slightly increased the power cost by 0.91 %, while enhancing overall system performance across technical, economic, environmental, and risk factors [25]. Ebadollahi et al. [26] optimized ORC and Kalina CHP systems for the Sabalan geothermal plant using a genetic algorithm. The ORC system achieved higher efficiency, while key parameters like condensation temperature (ORC) and ammonia concentration (Kalina) were crucial for optimization.

Integrating renewable energy systems for power and freshwater production is vital for remote areas, providing sustainable solutions to energy and water scarcity. This approach enhances both energy access and water availability through efficient use of resources [27]. In the Canary Islands, for example, harnessing wave energy to power seawater desalination plants offers a promising alternative to oil-based systems, improving both energy access and water availability while supporting environmental and socioeconomic goals [28]. Barone et al. [29] developed a dynamic simulation model in TRNSYS for optimizing energy systems on small, off-grid islands. Applied to El Hierro (Canary Islands), the model demonstrated that renewable energy sources could cover 85 % of electricity demand and 79 % of thermal needs, offering substantial economic savings. Moosavian et al. [30] model energy systems for Kish Island, Iran, using EnergyPLAN, highlighting a transition to renewables that reduces fossil fuel consumption by 36 % and CO_2 emissions by 0.7 million tons annually. The study aims for a fully renewable energy system by 2030, focusing on integrating renewable resources and reducing reliance on fossil fuels. In another study, an innovative system combining solar energy, a cascaded organic Rankine cycle, hydrogen production via electrolysis, and water desalination is proposed for island communities. The system generates 1.2 MW of electricity, 9.7 kg/h of hydrogen, and 33 kg/s of desalinated water, while reducing CO_2 emissions by 254 kg/h. The total system cost is 142 $/h, with a water cost of 33.2 Cent/m^3, providing a sustainable solution for energy and resource needs [31]. Mir and Bicer [32] discuss the increasing need for clean water, particularly in remote areas, and the potential of Electrodialysis for desalination and wastewater treatment. They highlight the integration of renewable energy sources like solar and wind to enhance the sustainability of these processes, especially for brackish water desalination.

Previous studies have shown that there has been an increasing focus on sustainable energy production from renewable sources. Combined generation systems have been introduced as an effective solution for sustainable systems. The integration of desalination systems has been reported as an effective way to enhance the performance of desalination systems and reduce their environmental impacts. The integration of energy systems for power and freshwater production is an effective strategy to reduce fuel consumption, minimize environmental impacts, and improve energy system performance. Additionally, optimizing energy systems is crucial for enhancing the efficiency of energy systems.

One of the weaknesses of previous studies is the limited focus on energy supply for remote areas, especially islands. Additionally, there has been a lack of new methods for analyzing energy systems, such as machine learning and advanced metaheuristic optimizers. The integration of desalination systems is another area that requires more in-depth studies. Comprehensive engineering analyses were rarely observed in previous research. Therefore, the present work introduces a combined power and freshwater generation system based on solar-biomass energy for the Canary Islands. The system utilizes a combination of a gas turbine (GT) cycle based on gasification, a steam Rankine cycle, and an organic Rankine cycle (ORC) for power generation. For freshwater production, the integration of MD-MED-RO systems is proposed. Machine learning is applied to analyze the subsystems of the proposed system. A comprehensive analysis of the proposed system is conducted, including techno-economic analysis and life cycle assessment, covering energy, exergy, exergoeconomic, and exergoenvironmental aspects. Furthermore, a multi-objective optimization is performed using new metaheuristic optimization algorithms (NSGA-III, MOMVO, and MOGOA). A dynamic analysis based on up-to-date data from the Canary Islands was conducted for the system, and the system was also examined from other perspectives, including sensitivity analysis. The innovations made in this research are as follows.

- Design of an innovative zero-emission solar-biomass energy-based system for power and freshwater generation for the Canary Islands.
- Integration of MD-MED-RO desalination systems for fresh water production.
- Application of machine learning for energy system analysis.
- Multi-objective optimization using advanced metaheuristic algorithms such as NSGA-III, MOMVO, and MOGOA.

2. Proposed system descriptions

The present study introduces an innovative cogeneration system for power, heat, and freshwater production, specifically designed for Las Palmas in Spain's Canary Islands. Located at 28.1°N latitude and −15.41°W longitude, Las Palmas benefits from high solar energy potential, making solar-based energy systems an ideal solution to address its water and energy demands.

The proposed system integrates solar energy and biomass to deliver sustainable and efficient performance. For power generation, a combination of the gas turbine cycle, steam Rankine cycle, and organic Rankine cycle is employed. Freshwater production is achieved through a hybrid desalination configuration, incorporating multi-effect distillation (MED), reverse osmosis (RO), and membrane distillation (MD). To mitigate environmental impacts, a carbon capture unit utilizing an amine solution is integrated into the power generation section, reducing greenhouse gas emissions.

The system harnesses solar energy via a solar tower to supply thermal energy and employs a steam-air gasification unit to utilize biomass resources. The process begins with ambient air entering an air compressor, where it is pressurized and preheated using the SHX1 heat exchanger, which receives thermal energy from the solar tower. The preheated air is then directed to a combustion chamber, where syngas from the gasification unit is used to produce high-temperature flue gas, driving the gas turbine to generate power.

The flue gas exiting the gas turbine retains sufficient thermal energy to generate additional power in the steam Rankine cycle. This cycle not only produces power through a heat recovery steam generator (HRSG) but also supplies the necessary thermal energy for the desalination and deaeration processes.

Freshwater production begins with the MED unit, which utilizes motive steam from the steam Rankine cycle to produce freshwater. The discharge cooling water from the MED system is divided into two streams: one stream supplies the RO unit, where freshwater is produced by overcoming osmotic pressure, and the other stream is directed to the MD unit. In the MD process, feedwater is heated and evaporated through direct contact membrane distillation (DCMD), producing freshwater by transferring heat to the permeate stream.

Although the flue gas exiting the heat recovery steam generator (HRSG) has lost most of its thermal energy during power and heat generation in the steam Rankine cycle, it retains sufficient potential to drive the organic Rankine cycle (ORC) for additional power production. The working fluid used in the ORC is R141B (1,1-Dichloro-1-fluoroethane), and the system responsible for recovering heat from the flue gas to generate power is the heat recovery vapor generator (HRVG).

After exiting the HRVG, the flue gas has no further thermal recovery potential due to the reduction in temperature and operational constraints, such as the dew point. At this stage, it is directed to the carbon capture unit for carbon dioxide removal. Inside the absorber column of the carbon capture unit, the flue gas undergoes heat and mass transfer with an amine solution, absorbing 90 % of the carbon dioxide content. The carbon-rich amine stream is then sent to the stripper column, where it is heated using a steam stream in the reboiler, releasing the absorbed carbon dioxide. The carbon dioxide is compressed and stored, while the regenerated amine solution is recycled back into the carbon capture process.

The solar tower provides thermal energy at 900 °C to support various sections of the system, including the Brayton cycle, gasification unit, and carbon capture unit. The heat transfer fluid (HTF) employed in the solar cycle is liquid sodium, ensuring efficient heat delivery.

The proposed system is designed to be self-sufficient and does not rely on an external consumer center. The electricity required for internal equipment such as compressors and pumps is supplied by the electricity generated within the system itself through the integrated turbines. If needed, backup electricity can be sourced from the local power grid; however, the system is primarily intended to operate independently, minimizing reliance on external energy sources.

Fig. 1 illustrates the proposed cogeneration system tailored for Las Palmas, Spain. Additionally, Table 1 presents the required input

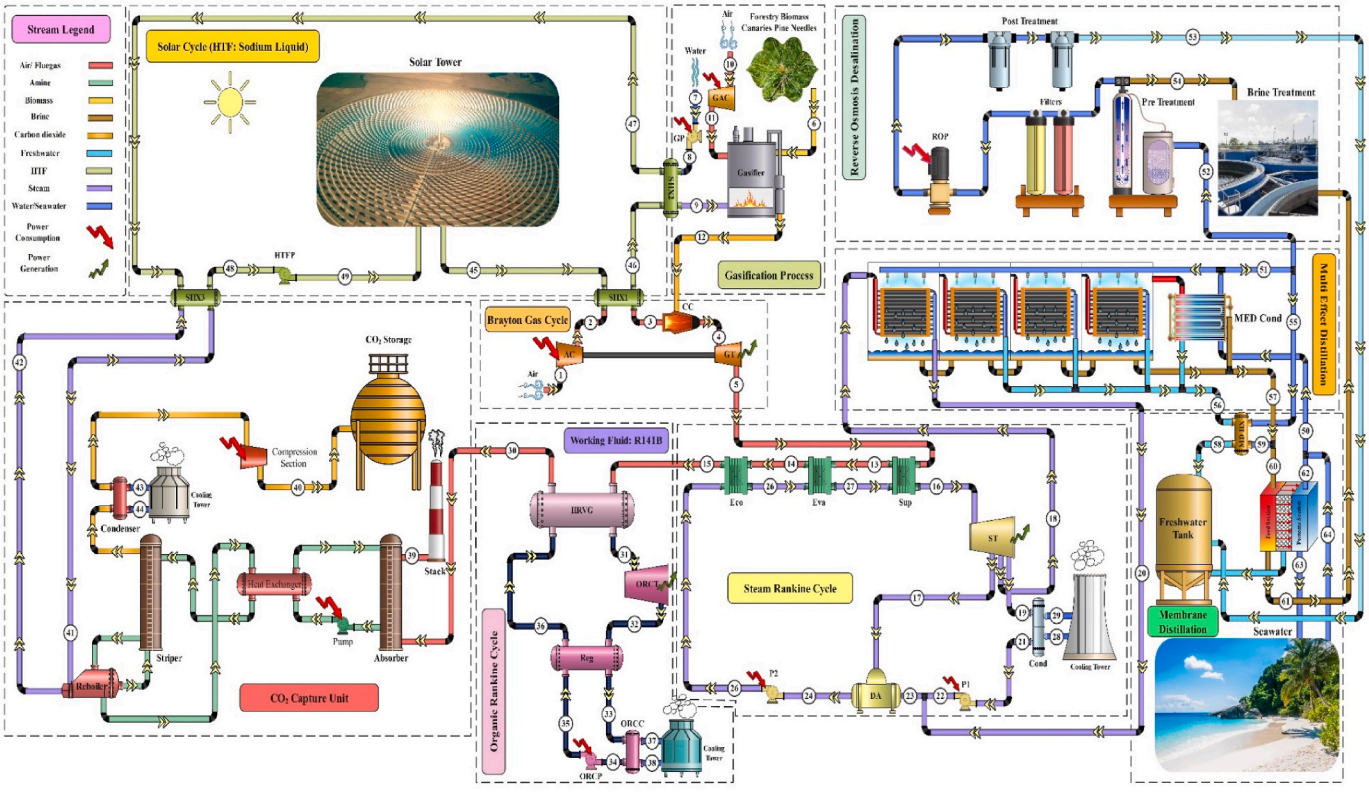

Fig. 1. Schematic of the solar-biomass cogeneration system proposed for the production of power and freshwater in the Canary Islands.

Table 1
Main input data for each section in the proposed cogeneration system.

Parameters	Unit	Value	Parameters	Unit	Value
GT Section			**Steam Rankine Section**		
Pressure ratio of air compressor	–	15.3	Steam turbine inlet pressure	bar	90
Gas turbine inlet temperature	°C	1149	Steam turbine inlet temperature	°C	450
Net power generation	MW	15	Deaerator pressure	bar	2.3
Air compressor isentropic efficiency	%	85	Steam turbine isentropic efficiency	%	85
Gas turbine isentropic efficiency	%	90	Pump isentropic efficiency	%	80
Combustion chamber efficiency	%	98	Condenser pressure	bar	0.5
Combustion chamber pressure drop	%	3	HRSG pinch point temperature	°C	20
ORC Section (Fluid: R141B)			Heat exchangers pressure drop	%	2
ORC turbine isentropic efficiency	%	85	Economizer sub cooled temperature	°C	5
ORC pump isentropic efficiency	%	80	Cooling water temperature Difference	°C	10
ORC turbine inlet temperature	°C	150	***CO_2 Capture Section*** [37]		
ORC turbine inlet pressure	bar	14	Carbon capture efficiency	%	90
ORC condenser pressure	bar	5	Carbon capture condenser pressure	bar	3
Flue gas stack temperature	°C	100	Carbon capture reboiler pressure	bar	5
Solar Tower Section (HTF: Sodium liquid)			***RO Desalination***		
Outlet temperature of solar tower	°C	900	RO feed pressure	bar	20
Outlet pressure of solar tower	bar	95	Isentropic efficiency of RO pump	%	85
Area of the heliostat mirror	m^2	10 × 10	***DCMD Desalination (membrane: PTFE)*** [35]		
Heliostat field efficiency	%	75	Porosity of membrane	%	85
Tower height	m	140	Membrane thickness	μm	45
Surface area of the solar receiver	m^2	33	Membrane Area	m^2	0.0572
Receiver tube outside diameter	m	0.04	Feed mass flow rate in each cells	L/hr	120
Receiver tube thickness	mm	1.25	Permeate mass flow rate in each cells	L/hr	180
Outlet temperature of SHX1	°C	800	***Biomass (Forestry type: Canary Pine Needles)*** [36]		
MED Desalination			Moisture content	%	10.5
Number of the effects	–	5	Carbon	%	49
Salinity of seawater	g/kg	36.7	Hydrogen	%	6.1
Sea water temperature rise at condenser	°C	15	Oxygen	%	4.04
Brine salinity outlet from MED section	g/kg	50	Nitrogen	%	1.20
Feed water mass flow rate entered to MED	kg/s	5	Biomass gasification pressure	bar	10

parameters for analyzing the performance of the proposed system. A set of main assumptions made in the present work are as follows.

- Heat losses in all heat exchangers and heat transfer equipment have been ignored.
- Gasification products consist solely of a mixture of hydrogen, methane, carbon monoxide, carbon dioxide, and nitrogen gases [33].
- The production of coal and tar during the gasification process is negligible and has been considered insignificant [33].
- The salinity of the seawater is assumed to be 36.7 g/kg, based on regional data [34].
- In the membrane distillation (MD) system, the membrane is made of polytetrafluoroethylene (PTFE) with a porosity of 85 % and a thickness of 45 μm [35].
- The biomass fuel used in the system is adapted to the conditions of the forest-type region, specifically Canary Pine Needles, with its composition obtained from Díaz et al. [36].

The feasibility of the proposed system has been evaluated through comprehensive techno-economic analysis and life cycle assessment (LCA) using MATLAB software. For the analysis of the gasification, MED, and CO_2 capture subsystems, machine learning techniques have been employed. Additionally, the multi-objective optimization of the proposed system has been conducted using three innovative metaheuristic algorithms. To derive the objective functions, a combination of deep learning neural networks and genetic algorithms was utilized.

3. Governing equations

As previously mentioned, the combined power and desalination system based on solar and biomass energy has been analyzed from the perspectives of energy, exergy, exergoeconomic, and exergoenvironmental aspects. Machine learning techniques have been applied to analyze certain components of the system. Furthermore, a dynamic analysis of the proposed system has been performed, tailored to the climatic conditions of the Canary Islands. Finally, three novel metaheuristic algorithms have been used to optimize the system's performance parameters. All analyses were conducted using MATLAB, while the machine learning models were implemented using Python. The following section presents the equations utilized for thermoeconomic analysis and life cycle assessment.

3.1. Thermoeconomic equations

This section provides the main equations required for the thermodynamic analysis of the proposed system. Initially, the equations necessary for the thermodynamic analysis of each subsystem are presented, followed by the economic equations.

3.1.1. Thermodynamic equations

The overall mass and energy balance for all steady-state equipment, neglecting kinetic and potential energy, can be calculated using the following equations [38].

$$\sum_{i=0}^{n} \dot{m}_{in} - \sum_{i=0}^{n} \dot{m}_{out} = 0 \tag{1}$$

$$\dot{Q} - \dot{W} = \sum_{i=0}^{n} \dot{m}_{out} h_{out} - \sum_{i=0}^{n} \dot{m}_{in} h_{in} \tag{2}$$

In the equations above, $\dot{m}$ represents the mass flow rate, $\dot{Q}$ represents heat transfer, and $\dot{W}$ represents power exchange.

Certain equipment requires additional auxiliary equations for thermodynamic analysis. The following presents some of the key equations necessary for the thermodynamic analysis of the gasification process, solar tower, desalination systems, and carbon capture systems.

- Gasification process

In the present study, biomass gasification using steam and air as agents has been utilized. The general chemical equation for this process is presented in Equation (3) [39].

$$CH_\alpha O_\beta N_Z + wH_2O + sH_2O + m(O_2 + 3.76N_2) \rightarrow x_1H_2 + x_2CO + x_3CO_2 + x_4H_2O + x_5CH_4 + \left(\frac{z}{2} + 3.76m\right)N_2 \quad (3)$$

The thermodynamic analysis of biomass gasification involves an iterative simultaneous solution to determine the composition of syngas. It is assumed that tar and char are negligible, and unknowns can be calculated by considering reforming and shifting reactions as the fastest reactions, along with the molar balance of elements. As mentioned earlier, solving these equations is time-consuming and requires an iterative process to ensure convergence [33].

In this regard, Khoshgoftar Manesh et al. [40] developed comprehensive correlations for various operational ranges using iterative solutions. They employed a smart combination of neural networks in machine learning and genetic programming in Python. The extracted correlations are presented in Table 2.

- Solar tower

The heat transferred from the heliostats surrounding the solar tower to the receiver can be determined using Equation (4) [41].

$$\dot{Q}_{receiver} = DNI \times A_{mirror} \times \eta_{field} \times \eta_{receiver} \quad (4)$$

Where DNI, A_{mirror}, η_{field}, and $\eta_{receiver}$ represent the direct normal radiation, solar field area, solar field efficiency, and receiver efficiency, respectively.

In the above equation, the necessary efficiency values are provided in Table 3. The heat loss from the heliostats and the absorbed heat from the solar field can be calculated using Equations (5) and (6).

$$\dot{Q}_{loss} = A_{receiver} \times \left[h_{air}\left(T_{ex} - T_0\right) - \sigma\,\varepsilon\left({T_{receiver}}^4 - {T_0}^4\right)\right] \quad (5)$$

$$\dot{Q}_{abs} = \dot{Q}_{receiver} - \dot{Q}_{loss} \quad (6)$$

In the above equations, h_{air} is the air convection coefficient, σ is the Boltzmann constant, and ε is the emissivity. T_{ex}, $T_{receiver}$, and T_0 represent the outlet temperature of the receiver, the receiver temperature, and the ambient temperature, respectively. Other related equations for heliostat design modeling can be derived from Ref. [42].

Table 2
The equations for the biomass gasification process with steam and air agents, as extracted by GP-ANN [40].

Descriptions	Equations
CH_4 mole fraction	$y_{ch_4} = 0.340H^2 + 0.002P_GC^2 + 0.0007{P_G}^2MC^2 - 0.0004 - 0.016P_GHO - 0.521CH^2$
CO mole fraction	$y_{CO} = 0.092 + 0.079H + 0.016O - 0.0004P_G - 0.018C - 0.131N - 0.168MC$
CO_2 mole fraction	$y_{CO_2} = 0.115 + 0.150C + 0.043MC + 0.0002P_G - 0.030O - 0.905H$
H_2 mole fraction	$y_{H_2} = 0.156 + 0.619H + 0.192C - 0.041N - 0.2O - 0.851CH$
H_2O mole fraction	$y_{H_2O} = 0.249 + 0.472O + 0.397H + 0.330MC - 0.052N - 0.420C$
N_2 mole fraction	$y_{N_2} = 0.357 + 0.264H + 0.152C + 0.114N - 0.206MC - 0.252O$
Syngas temperature	$T_G = 861.126 + 2536.553H + 915.683O - 2.572P_G - 412.292MC - 424.420N - 1051.946C$
Biomass mass flowrate	$\dot{m}_{Bio} = 0.280\dot{m}_{Syngas} - 0.072\dot{m}_{Syngas}C - 0.263\dot{m}_{Syngas}MC - 0.435\dot{m}_{Syngas}H$
Steam mass flowrate	$\dot{m}_{Steam} = 0.750 - 0.132\dot{m}_{Syngas} + 0.209\dot{m}_{Syngas}O - 0.138\dot{m}_{Syngas}MC - 21.072CH$
Air mass flowrate	$\dot{m}_{Air} = 0.110 + 4.437H + 0.773C + 0.114\dot{m}_{Syngas} - 1.154MC - 1.542N - 1.717O$

Table 3
Solar field specifications [43].

Parameters	Specifications
Location of field	Canary Islands, Spain
Latitude	28.1 °N
Longitude	−15.41 °W
Receiver area	17.33 m^2
Total field area	41.14 Hectares
Number of mirrors	1400
Tower height	100 m
η_{cosine}	0.82
$\eta_{reflectivity}$	0.90
$\eta_{blocking}$	1
$\eta_{shading}$	1
$\eta_{Intercept}$	0.85
$\eta_{attenuation}$	0.92
$\eta_{receiver}$	0.56

- Multi-effect distillation (MED)

The thermodynamic analysis of MED desalination includes mass and energy balances for each of the effects, feedwater heaters, condensers, and the entire system. This process requires a complex and time-consuming analysis that involves the simultaneous solution of heat transfer and mass transfer equations for the system. For simplicity, in this stage, machine learning equations extracted by Mousavi Rabeti et al. [4] have been used. These equations are provided in Table 4.

- Reverse osmosis (RO)

The thermodynamic equations required for the analysis of the RO desalination system are presented in Table 5. Using these equations, the mass flow rate of the freshwater, feed water, and brine can be calculated. It should be noted that the feed water input is equal to the cooling water output from the MED system, so this acts as an auxiliary equation alongside the other equations.

- Membrane distillation

Vapor transfer from the feed side to the permeate side of the membrane occurs due to the pressure gradient driven by the temperature difference between the two sides. The mass transfer can be expressed as a linear relationship with the vapor pressure difference across the membrane, represented by Ref. [35]:

$$J = C_m(P_1 - P_2) \quad (7)$$

Table 4
The equations for the MED desalination, as extracted by GP-ANN.

Descriptions	Equations
Distilled mass flowrate	$\dot{\boldsymbol{m}}_{\boldsymbol{d}} = 14.392 + 0.0270\,\dot{\boldsymbol{m}}_{\boldsymbol{f}}\boldsymbol{x}_{\boldsymbol{B}} - 0.215\,\boldsymbol{x}_{\boldsymbol{sw}} - 0.853\,\boldsymbol{n} - 0.020\,\boldsymbol{x}_{\boldsymbol{sw}}\dot{\boldsymbol{m}}_{\boldsymbol{f}} - 0.0001\dot{\boldsymbol{m}}_{\boldsymbol{f}}\boldsymbol{x}_{\boldsymbol{B}}^{\boldsymbol{2}}$
Specific area	$\boldsymbol{SA} = 17567.638 + 0.001\,\boldsymbol{T}_{\boldsymbol{en}}^{\boldsymbol{4}} + 0.926\,\boldsymbol{n}\,\boldsymbol{T}_{\boldsymbol{en}}^{\boldsymbol{2}} - 495.041\boldsymbol{T}_{\boldsymbol{en}} - 672.865\,\boldsymbol{n} - 0.013\,\boldsymbol{n}\,\boldsymbol{T}_{\boldsymbol{en}}^{\boldsymbol{3}}$
1st effect steam mass flowrate	$\dot{\boldsymbol{m}}_{\boldsymbol{se1}} = 5.687 + 0.255\,\dot{\boldsymbol{m}}_{\boldsymbol{f}} + 0.052\,\boldsymbol{n}^{\boldsymbol{2}} + 0.001\,\dot{\boldsymbol{m}}_{\boldsymbol{f}}\,\boldsymbol{n}^{\boldsymbol{2}} - 0.152\frac{\boldsymbol{x}_{\boldsymbol{sw}}\dot{\boldsymbol{m}}_{\boldsymbol{f}}}{\boldsymbol{x}_{\boldsymbol{B}}} - 1.150\,\boldsymbol{n} - 0.019\,\boldsymbol{n}\,\dot{\boldsymbol{m}}_{\boldsymbol{f}}$
Recovery ratio	$\boldsymbol{RR} = 1.208 - 0.009\,\boldsymbol{n} - 0.010\,\boldsymbol{x}_{\boldsymbol{sw}} - 0.080\,\boldsymbol{x}_{\boldsymbol{sw}} \times 0.554^{0.062\boldsymbol{x}_{\boldsymbol{B}}}$
Seawater mass flowrate	$\dot{\boldsymbol{m}}_{\boldsymbol{sw}} = 627.444 + \dot{\boldsymbol{m}}_{\boldsymbol{f}} + 0.049\,\dot{\boldsymbol{m}}_{\boldsymbol{f}}\boldsymbol{x}_{\boldsymbol{B}} + 4.348\,\boldsymbol{n}^{\boldsymbol{2}} - 6.946\,\boldsymbol{x}_{\boldsymbol{sw}} - 61.214\,\boldsymbol{n} - 0.220\,\boldsymbol{n}\dot{\boldsymbol{m}}_{\boldsymbol{f}} - 0.504\,\boldsymbol{n}\,\boldsymbol{T}_{\boldsymbol{en}}$
Cooling water discharge mass flowrate	$\dot{\boldsymbol{m}}_{\boldsymbol{cwd}} = 111.781\,\boldsymbol{n} + 25.198\,\boldsymbol{T}_{\boldsymbol{en}} + 0.5325\,\dot{\boldsymbol{m}}_{\boldsymbol{f}} + 0.139\,\boldsymbol{T}_{\boldsymbol{en}}\,\boldsymbol{x}_{\boldsymbol{B}} + 3.447\,\boldsymbol{n}^{\boldsymbol{2}} - 872.493 - 0.094\,\boldsymbol{x}_{\boldsymbol{sw}}\boldsymbol{x}_{\boldsymbol{B}} - 4.210\,\boldsymbol{n}\boldsymbol{T}_{\boldsymbol{en}}$
Distilled temperature	$\boldsymbol{T}_{\boldsymbol{D}} = 360.992 + 0.105\,\boldsymbol{x}_{\boldsymbol{B}} + 0.160\,\boldsymbol{T}_{\boldsymbol{en}}^{\boldsymbol{2}} + 6.8604 \times 10^{-8}\boldsymbol{x}_{\boldsymbol{B}}\boldsymbol{T}_{\boldsymbol{en}}^{\boldsymbol{4}} - 14.237\boldsymbol{T}_{\boldsymbol{en}} - 4.344 \times 10^{-6}\,\boldsymbol{x}_{\boldsymbol{B}}\,\boldsymbol{T}_{\boldsymbol{en}}^{\boldsymbol{3}} - 1.183 \times 10^{-8}\,(\boldsymbol{x}_{\boldsymbol{B}}\boldsymbol{T}_{\boldsymbol{en}})^2$

Table 5
Related equation of modeling RO desalination [44].

Equation	Description
$RR = \frac{\dot{m}_D}{\dot{m}_F}$	Recovery Ratio
$RR = RR\|_{T=25} \times \frac{J_w}{J_w\|_{T=25}}$	Recovery Ratio
$\dot{m}_F = \dot{m}_D + \dot{m}_B = \dot{m}_{cwd\_MED}$	Mass flow rate of feed
$J_w = \frac{D_w C_w V_w}{RTe[K]}\{(P_F - P_D) - (\pi_F - \pi_D)\}$	specific mass flow rate of water
$\pi_i = \frac{385 \times sal_i \times T_i}{0.14507(1000 - 10sal_i)}$	Osmosis Pressure of seawater and distilled
$D_w = \frac{kT}{3\pi_F \mu_w d_s}$	Coefficient of diffusion of water in membrane
$sal_B = \frac{sal_F}{1 - RR}$	Salinity of brine
$h_B = \frac{h_F - RR \times h_D}{1 - RR}$	Enthalpy of brine
$\mu_w = 4.23 \times 10^{-5} + [0.157(T_F + 64.993)^2 - 91.296]^{-1}$	Dynamic viscosity of water

Here, J represents the mass flux, C_m denotes the membrane distillation (MD) coefficient, and P_1 and P_2 are the partial pressures of water vapor at the membrane surface temperatures T_1 and T_2, respectively.

The MD coefficient (C_m) depends on the Knudsen number and can be calculated under three distinct conditions.

Partial pressures of water vapor at the membrane surface temperatures can be calculated by following equation:

$$P = \exp\left(23.238 - \frac{3841}{T - 45}\right) \tag{8}$$

The heat transfer mechanisms in membrane distillation (MD) can be outlined as follows:

Convective heat transfer occurs as thermal energy is transferred from the feed side to the membrane surface through the boundary layer.

$$q_f = h_f(T_f - T_1) \tag{9}$$

where q_f is the feed heat flux (W/m^2) and h_f is the heat transfer coefficient (W/m^2 K).

The heat flux across the membrane consists of two components: conduction heat transfers through the membrane's solid material, expressed as $k_m \frac{dT}{dx}$, and latent heat transfer carried by water vapor through the membrane pores, represented as JH_v.

$$q_m = JH_v + k_m \frac{dT}{dx} \tag{10}$$

H_v represents the enthalpy of vaporization of water, calculated at the mean temperature $\frac{T_1+T_2}{2}$. The second component corresponds to the conduction heat loss through the membrane material.

Finally, heat is transferred from the permeate boundary layer to the permeate water through convection.

$$q_p = h_p(T_2 - T_p) \tag{11}$$

At steady state:

$$q_f = q_m = q_p \tag{12}$$

The overall heat transfer coefficient can be determined using the following equation:

$$U = \left[\frac{1}{h_f} + \frac{1}{\frac{k_m}{\delta_m} + \frac{JH_v}{T_1 - T_2}} + \frac{1}{h_p}\right]^{-1} \tag{13}$$

The rate of total heat transferred through the membrane is as follows:

$$q_t = U(T_f - T_p) \tag{14}$$

The feed flow energy balance is as follows:

$$q_f = \dot{m}_f c_p(T_f - T_p) \tag{15}$$

The computational algorithm for the thermodynamic analysis of DCMD desalination can be derived using the research work by Ali et al. [45].

- CO_2 capture unit

The thermodynamic analysis of the carbon dioxide capture unit is considered a complex energy analysis due to the interdependence of the equations and the large number of components involved. If an amine absorption and desorption tower is assumed, adding a tray to these towers introduces numerous mass balance equations, complicating the thermodynamic analysis of these systems. Therefore, Khani et al. [37] developed comprehensive correlations for this unit by simulating the system in the Thermoflex software and examining different operating conditions. These correlations include the mass flow rate of carbon dioxide, the required input heat for the unit in the reboiler, and the electrical power demand, all of which were extracted using machine learning modeling.

$$\dot{m}_{CO_{2out}} = \dot{m}_{CO_{2in}} \times \eta_{CO_2\ Capture} \tag{16}$$

$$\dot{Q}_{in_{CO_2\ Capture}} = 4.028 \times \left(\eta_{CO_2\ Capture} \times 100 - 0.002\right) \tag{17}$$

$$\dot{W}_{CO_2\ Capture} = 0.439 \times \left(\eta_{CO_2\ Capture} \times 100 - 0.0002\right) \tag{18}$$

3.1.2. Exergy equations

This section presents the equations for exergy analysis. The overall exergy balance for steady-state systems, assuming the neglect of kinetic and potential energy, is given by the following equations.

$$\dot{E}x_Q + \sum_i \dot{m}_i ex_i = \sum_e \dot{m}_e ex_e + \dot{E}x_W + \dot{E}x_D \tag{19}$$

The exergy of the flow includes both physical exergy and chemical exergy. In the proposed system, the chemical exergy is defined for biomass, flue gas, seawater, and brine, and the corresponding relationships are provided below.

$$ex_{ph} = (h - h_0) - T_0(s - s_0) \tag{20}$$

The chemical exergy of the biomass is calculated from the following equation:

$$ex^{ch}_{Bio} = \beta \times LHV_{Bio} \tag{21}$$

LHV_{Bio} is the lower heating value of a biomass, calculated for in Ref. [46], and the beta for biomass fuels is as follows [47].

$$\beta = \frac{1.0414 + 0.0177\left[\frac{H}{C}\right] - 0.3328\left[\frac{O}{C}\right]\left(1 + 0.0737\left[\frac{H}{C}\right]\right)}{1 - 0.4021\left[\frac{O}{C}\right]} \tag{22}$$

The chemical exergy of the mixture will be calculated using the following equation, which references [48] for the syngas chemical exergy of each component and [49] for the flue gas.

$$ex^{mix}_{ch} = \left[\sum_{i=1}^{n} X_i ex^{ch_i} + RT_0 \sum_{i=1}^{n} X_i \ln X_i\right] \tag{23}$$

X_i is the molar fraction of each component in the mixture. The chemical exergy of saline water can be calculated using Equation (24) below [50].

$$\bar{ex}^{ch}_{sw} = mf_s(\mu^*_s - \bar{\mu}^0_s) - mf_w(\mu^*_w - \bar{\mu}^0_w) \tag{24}$$

In the above relation, mf_s is the mass fraction of salt in seawater, and μ^*_s

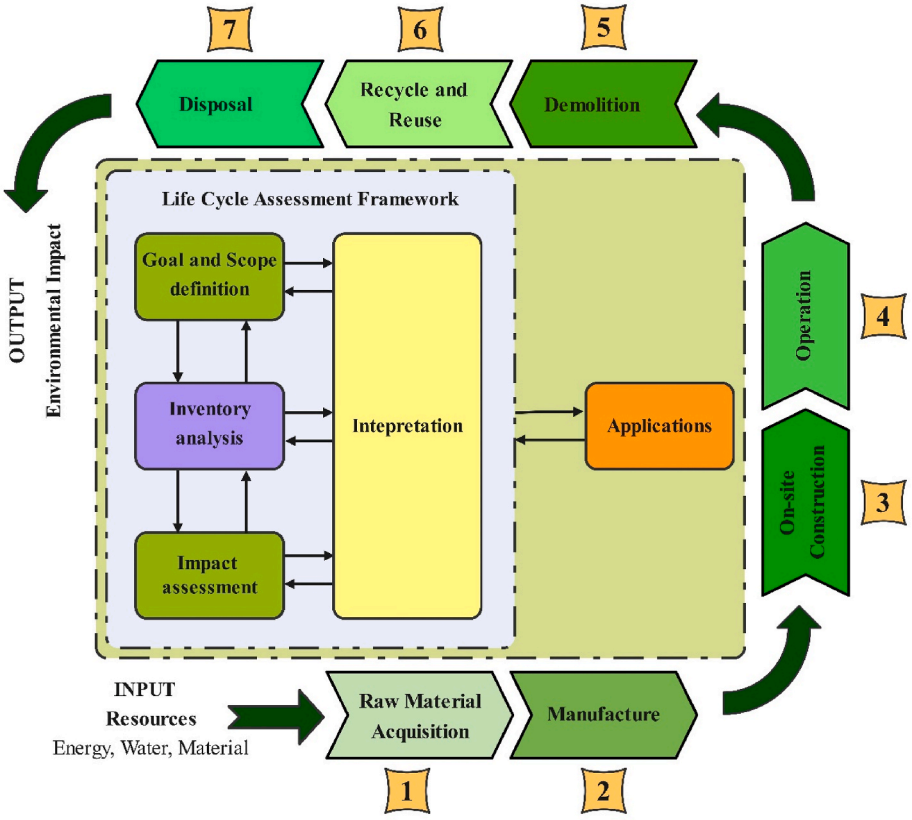

Fig. 2. The LCA framework and Life Cycle Stages.

is the chemical potential of salt in seawater at a restricted dead state, while μ_w^* refers to the chemical potential of water.

The solar exergy can be seen in Equation (25) [51].

$$\dot{E}x_{solar} = \dot{Q}_{solar}\left(1 - \frac{4}{3}\frac{T_a}{T_{sun}}(1 - 0.28\,ln(f_{dil}))\right) \tag{25}$$

Where $\dot{Q}_{solar}$ is the heat reaches the heliostat, T_a is the ambient temperature and T_{sun} is sun temperature ($T_{sun} = 5800\,K$), and f_{dil} is the Dilution factor with the value of $f_{dil} = 1.3 \times 10^{-5}$.

Exergy destruction of each component that represents its irreversibility is defined as the following equation.

$$\dot{E}x_{D,k} = \dot{E}x_{F,k} - \dot{E}x_{P,k} \tag{26}$$

In Equation (26), $\dot{E}x_{F,k}$ is the fuel exergy of each equipment, and $\dot{E}x_{P,k}$ is the product exergy that is considered as a target in them.

Therefore, the exergy efficiency of each equipment, which indicates the quality of energy performance of them, is defined as follows:

$$\psi_k = \frac{\dot{E}x_{P,k}}{\dot{E}x_{F,k}} \tag{27}$$

3.1.3. Economic analysis equations

The feasibility study of cogeneration and polygeneration systems is intrinsically tied to their economic evaluation; without this critical assessment, even the most promising systems remain inadequately analyzed [38]. Various economic analyses, such as thermoeconomic, exergeoeconomic, and environmental economic evaluations, are frequently applied, with the first two being particularly common. Each type of analysis serves distinct purposes. For example, thermoeconomic analysis emphasizes calculating equipment costs, payback period (PP), internal rate of return (IRR), and net present value (NPV) [52,53]. Conversely, exergeoeconomic analysis focuses on evaluating the costs of streams, fuel consumption, product generation, and exergy destruction in equipment, offering a more comprehensive insight into the economic aspects of the system, its processes, and components [54].

The overall exergeoeconomic balance is defined as follows [55]:

$$\sum c_i \dot{E}x_i + c_q \dot{E}x_Q + \dot{Z}_k = \sum c_e \dot{E}x_e + c_w \dot{E}x_W \tag{28}$$

Where, c_i, c_e, c_q, and c_w are cost per exergy for inlet steam, outlet steam, heat transfer, and work. $\dot{Z}_k$ also is cost investment rate of component that can be calculated using equation (29).

$$\dot{Z}_k = \frac{PEC_k \times CRF \times \varphi}{3600 \times N} \tag{29}$$

In above equation, PEC_k is purchase equipment cost of component, CRF is cost recovery factor, φ is maintenance factor (1.06), and N operation working hours in year (8000 h for all equipment and 5000 for solar cycle). The CRF can be calculated by equation (30). PEC_k is also calculated for the equipment based on the thermodynamic parameters of the operation, as reported for all the system's equipment in Table A1 of Appendix section.

$$CRF = \frac{i \times (1+i)^n}{(1+i)^n - 1} \tag{30}$$

In Equation (30), i and n are interest rate (10 %) and number of a lifetime year (25 years), respectively.

The payback period of whole system can be calculated by following equation:

$$PP = \frac{FC}{ANS} \tag{31}$$

Where, FC is fixed cost of whole system and ANS is annual net saving cost.

The formula for NPV is given by Equation (32) [56,57].

$$NPV = \sum_{m=1}^{n} (IF_m \times RDF_m \times AS) - FC \quad (32)$$

Where IF_m represents the inflation factor for year m, RDF_m represents the real discount factor for year m, AS denotes the annual net saving money, and FC refers to the fixed costs.

3.2. Life cycle assessment (LCA)

Environmental factors play a crucial role in designing energy systems. Various methods are employed to assess their environmental impact, such as evaluating pollutant emissions, conducting life cycle assessments (LCA), calculating carbon and water footprints (CF and WF), and estimating the environmental effects of emissions generated by these systems [40]. Among these, LCA stands out as the most comprehensive approach.

Life Cycle Assessment (LCA) is a structured methodology for evaluating the environmental impacts of a product, process, or system throughout its entire life cycle, encompassing stages such as raw material extraction, production, usage, and eventual disposal or recycling. By analyzing the environmental effects at each phase, LCA provides a holistic understanding of the overall environmental footprint [58].

In the context of energy systems, LCA proves invaluable for comparing the environmental impacts of various energy sources, including fossil fuels and renewables [59]. It aids in determining the total carbon footprint of different energy technologies, assessing resource consumption such as water and minerals, pinpointing critical stages with significant environmental impacts—like raw material extraction or operational phases—and offering guidance for sustainable energy production and policy development aimed at cleaner, more efficient solutions.

LCA consists of four key components [60]. First, the Goal and Scope Definition establishes the study's purpose, system boundaries, and functional unit (e.g., 1 kW-hour of electricity). Second, the Inventory Analysis gathers data on energy, material inputs, and emissions across all life cycle stages. Third, the Impact Assessment evaluates potential environmental effects, including global warming potential, resource depletion, and pollution. Finally, the Interpretation phase analyzes the findings to identify areas for improvement, explore trade-offs, and recognize limitations, ultimately providing actionable insights for enhancing environmental sustainability. Fig. 2 illustrates the Life Cycle Assessment (LCA) Framework and its associated Life Cycle Stages.

Life Cycle Assessment (LCA) is a structured and internationally standardized methodology, governed by ISO 14040 and ISO 14044 standards, for evaluating the environmental impacts of a product, process, or system throughout its life cycle. These ISO standards provide a consistent framework to ensure transparency, reproducibility, and scientific rigor in the assessment process.

The methodology includes four main phases: goal and scope definition, inventory analysis, impact assessment, and interpretation. In this study, the LCA was conducted using SimaPro 9.3 software with the Ecoinvent 3.8 database. The Eco-indicator 99 (EI-99) method was selected for impact assessment due to its comprehensive aggregation of environmental effects into three main damage categories: Human Health, Ecosystem Quality, and Resource Depletion.

While LCA offers a comprehensive perspective on environmental impacts, it does not account for the quality of energy used or the thermodynamic performance of the system. To bridge this gap, an exergoenvironmental assessment is employed. This approach combines exergy analysis (which considers the quality and usability of energy) with environmental impact assessment, providing a deeper understanding of the environmental cost per unit of useful energy.

According to Meyer [61], exergoenvironmental analysis quantifies the environmental impact of each system component by assigning environmental impact rates to exergy streams throughout the process. This method enables the identification of components with the highest environmental burden and supports sustainable design optimization.

The overall exergoenvironmental balance for the equipment is calculated using equation (33).

$$\sum b_i \dot{E}x_i + b_q \dot{E}x_Q + \dot{Y}_k = \sum b_e \dot{E}x_e + b_w \dot{E}x_W \quad (33)$$

Where, b_i, b_e, b_q, and b_w are environmental impact per exergy for inlet steam, outlet steam, heat transfer, and work. $\dot{Y}_k$ also is environmental impact rate of component that can be calculated using equation (34).

$$\dot{Y}_k = \frac{Weight_k \times lbm_k}{3600 \times N \times n} \quad (34)$$

In equation (25), $Weight_k$ is components weight that is calculated in Table A1 of Appendix. lbm_k is the environmental impact per weight of components that rely on the composite material of the equipment, which can be calculated using Table 6.

Table 6
Environmental impacts of some component based on LCA [62].

Component	Material Composition	Eco' 99 Indicator (mPts/kg)	Material (mPts/kg)	Process (mPts/kg)	Disposal (mPts/kg)	Total (mPts/kg)
Compressors	Steel 33,33 %	86	130	11.7	−70.0	71.7
	Steel low alloy 44,5 %	110				
	Cast iron 22,22 %	240				
Combustion Chamber	Steel 33,34 %	86	635	20.0	−70.0	585
	Steel high alloy 66.66 %	910				
Turbines	Steel 25 %	86	704	12.1	−70.0	646
	Steel high alloy 75 %	910				
Pumps	Steel 35 %	86	186	16.9	−70.0	132.8
	Cast iron 65 %	240				
Gasifier	Steel 100 %	86	86	12.1	−70.0	28.0
Deaerator	Steel 100 %	86	86	12.1	−70.0	28.0
Condenser	Steel 100 %	86	86	12.1	−70.0	28.0
Heat Exchangers	Steel 25 %	86	696	12.1	−70.0	28.0
	Steel high alloy 75 %	910				
Super Heater	Steal 25 %	86	704	12.1	−70.0	646
	Steel high alloy 75 %	910				
Evaporator	Steel 100 %	86	86	12.1	−70.0	28.0
Economizer	Steel 100 %	86	86	12.1	−70.0	28.0
Solar Tower	Steel 98 %	86	85	7.3	−69.0	23.2
	Glass 2 %	58				
CO_2 capture	Steel 100 %	86	86	12.1	−70.0	28.0

To analyze the life cycle of desalination systems, the following relationships can be derived based on Raluy et al. [63] and Liang et al. [64].

$$\dot{Y}_{RO} = 0.0195 \times \frac{\rho \times \dot{W}_{RO}}{3600 \times \dot{m}_{RO-distilled}} + 0.00595 \left(\frac{mPts}{h.\ m^3}\right) \quad (35)$$

$$\dot{Y}_{MED} = 1.277 \left(\frac{mPts}{h.\ m^3}\right) \quad (36)$$

$$\dot{Y}_{MD} = 0.7 \left(\frac{Pts}{m^3}\right) \quad (37)$$

3.3. Multi-objective optimization

Mathematical optimization is a process in which the best solution is selected from a set of feasible options for a specific problem. It is widely applied across various quantitative scientific fields, such as computer science, engineering, operations research, and economics. Optimizing energy systems is a key area of focus, as it helps reduce fuel consumption, lower operating costs, and minimize environmental impacts. Many algorithms have been developed to address engineering optimization challenges, with metaheuristic algorithms being particularly noteworthy. These algorithms are inspired by natural processes and, compared to traditional mathematical methods, offer the advantage of optimizing problems with high accuracy in shorter timeframes.

In the present work, three novel metaheuristic algorithms have been utilized to optimize the performance of the proposed system, with a three-objective optimization approach. The selected decision variables and the considered objective functions are presented in accordance with Table 7.

Table 7
The specifications of the decision variables and the objective functions for the multi-objective optimization of the proposed system.

No.	Parameters	Symbol	Unit	Lower bound	Upper bound
DV_1	Pressure ratio of air compressor	rp_{AC}	–	10	16
DV_2	Gas turbine inlet temperature	TIT_{GT}	°C	1100	1200
DV_3	Net power generation from the GT package	$\dot{W}_{Net,Gt}$	kW	14500	15500
DV_4	MED last effect temperature	$T_{e_{MED}}$	°C	55	65
DV_5	MED brine outlet salinity	$x_{B_{MED}}$	%	45	55
DV_6	Outlet temperature of sodium liquid from SHX1	$T_{out,SHX1}$	°C	550	650
DV_7	RO feed pressure	$P_{f,RO}$	bar	15	25
OF_1	Cogeneration efficiency	η_{Cogen}	%	–	–
OF_2	Payback period	PP	Year	–	–
OF_3	Total environmental impact rate	$\dot{B}_{tot}$	mPts/s	–	–

- Non-dominated Sorting Genetic Algorithm III (NSGA-III)

NSGA-III (Non-dominated Sorting Genetic Algorithm III) is an evolutionary algorithm designed for many-objective optimization problems, typically involving three or more objectives. It builds upon NSGA-II by introducing a reference-point-based approach to improve the distribution of solutions along the Pareto front. This approach ensures that the population members are not only non-dominated but also close to predefined reference points, enhancing solution diversity. NSGA-III efficiently manages the challenges of many-objective problems, such as the exponential increase in nondominated solutions, and avoids overwhelming the population with too many candidates. The algorithm preserves better diversity among solutions by guiding the search process using reference points, making it more effective than traditional methods in high-dimensional spaces. NSGA-III has shown robust performance across various test problems and has outperformed other evolutionary multi-objective optimization algorithms like MOEA/D in certain scenarios. It is particularly suitable for problems with a high number of objectives (up to 15 or more) and is valuable for complex real-world applications. The algorithm provides a balanced approach, focusing on both convergence towards optimal solutions and maintaining diversity in the solution set, ensuring high-quality results. Its success in practical applications further highlights its versatility and effectiveness, making NSGA-III a significant advancement in evolutionary multi-objective optimization [65]. The computational flowchart of NSGA-III is presented in Fig. 3 [66].

- Multi-Objective Multi-Verse Optimization (MOMVO)

MOMVO (Multi-Objective Multi-Verse Optimizer) is an extension of the Multi-Verse Optimizer (MVO) designed specifically for multi-objective optimization problems. It enhances the original MVO by incorporating an archive and updating mechanism, which improves the

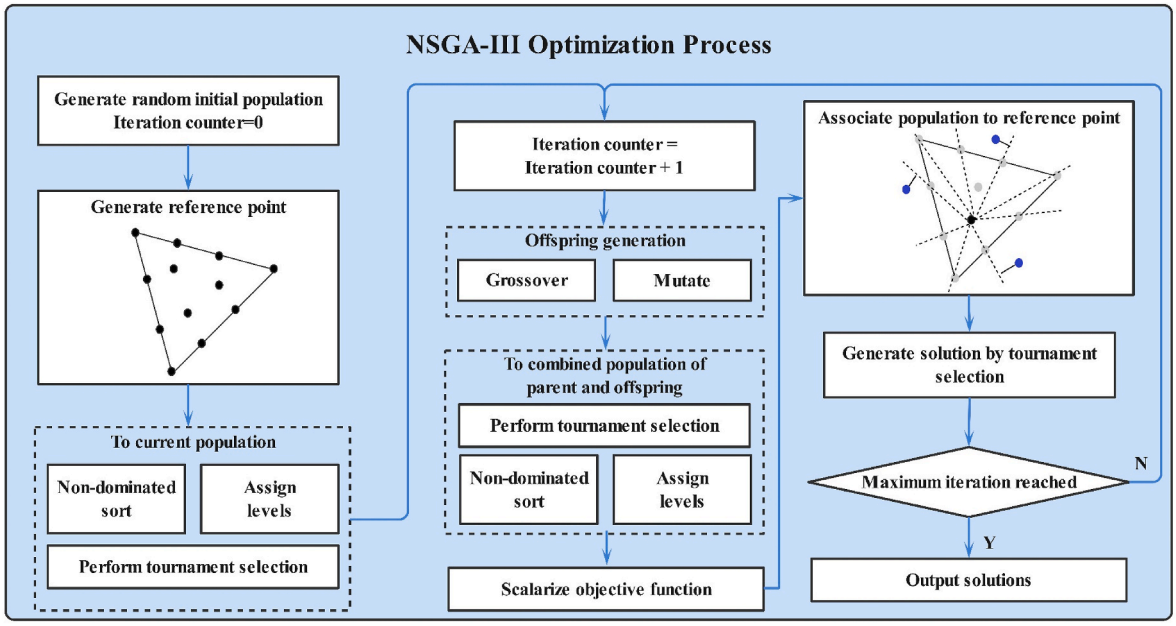

Fig. 3. The NSGA-III flowchart [66].

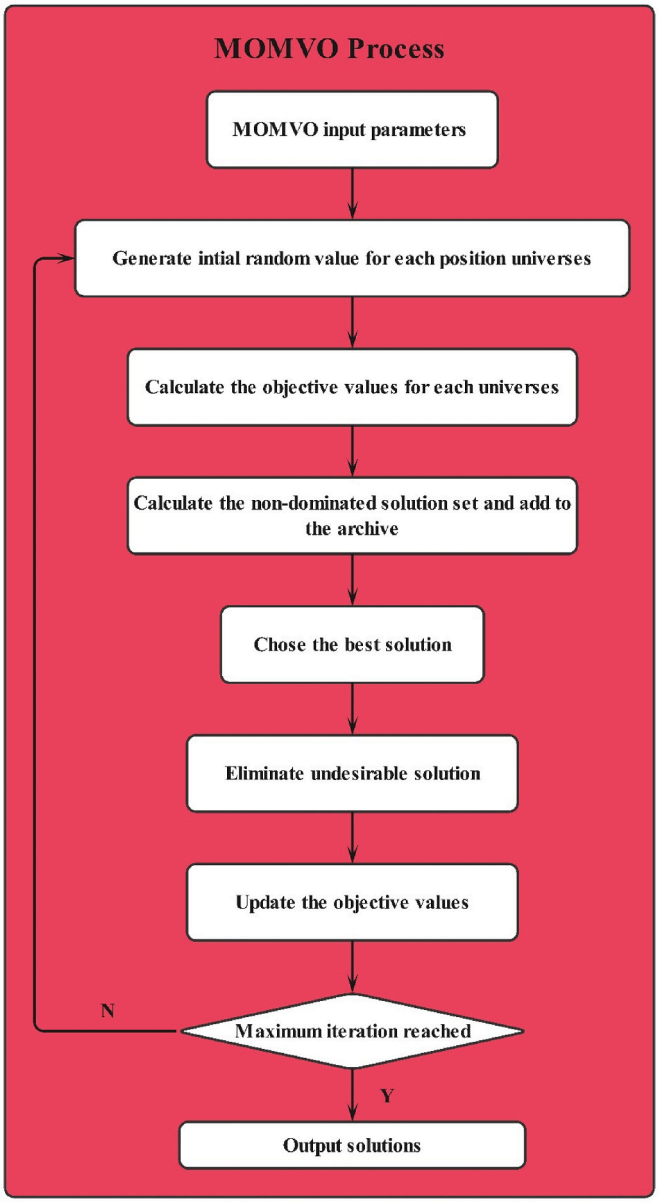

Fig. 4. The MOMVO flowchart [68].

coverage of Pareto optimal solutions. This allows MOMVO to navigate the multi-objective search space effectively, converging towards optimal solutions while preserving a diverse set of results. The algorithm excels in improving Pareto front coverage by storing and updating non-dominated solutions through the archive, ensuring a wide exploration of optimal solutions. It has demonstrated robust performance in various case studies, including both unconstrained and constrained multi-objective problems, outperforming other established algorithms like NSGA-II and MOPSO. MOMVO is also adept at handling constraints, addressing challenges that many other multi-objective optimization algorithms face. It is versatile, applicable to a wide range of engineering design problems, and capable of optimizing multiple objectives simultaneously, making it suitable for real-world applications. The algorithm yields high-quality solutions by promoting diversity and using the archive mechanism to explore good trade-offs among competing objectives, while also reducing human involvement by automating the optimization process and minimizing the potential for manual errors. In conclusion, MOMVO is an effective tool for complex multi-objective optimization problems, offering a unique approach to maintaining diversity and managing constraints [67]. The computational flowchart of MOMVO is presented in Fig. 4 [68].

- *Multi-objective Grasshopper Optimization Algorithm (MOGOA)*

The Multi-Objective Grasshopper Optimization Algorithm (MOGOA) is an advanced adaptation of the Grasshopper Optimization Algorithm (GOA) tailored for solving multi-objective optimization problems. Inspired by the natural swarming behavior of grasshoppers, MOGOA simulates their social interactions and dynamic movement patterns to efficiently explore the search space and find diverse Pareto-optimal solutions.

By employing mechanisms that balance exploration and exploitation, MOGOA maintains diversity among solutions and ensures convergence to the optimal Pareto front. The algorithm uses adaptive control parameters to adjust the grasshopper population's behavior, enhancing its capability to handle conflicting objectives. Its simplicity and effectiveness make it suitable for a wide range of applications, including engineering design and resource allocation.

Compared to traditional multi-objective algorithms, MOGOA offers robust performance in high-dimensional search spaces, ensuring well-distributed solutions across the objective spectrum. It automates the optimization process, minimizing manual intervention and providing reliable trade-offs between objectives, making it a valuable tool for complex decision-making scenarios [69]. The computational flowchart of MOGOA is presented in Fig. 5 [70].

4. Research methodology

Fig. 6 illustrates the comprehensive research methodology developed for the solar-biomass cogeneration system, tailored to meet the energy and freshwater demands of the Canary Islands. This methodology integrates advanced modeling and optimization techniques to ensure a balance between thermodynamic efficiency, economic feasibility, and environmental sustainability. It is divided into two primary stages: System Modeling and Optimization, covering all aspects necessary for the successful deployment of the proposed system.

4.1. Proposed system modeling

This stage provides a systematic evaluation of the proposed system through a sequence of interconnected analyses. These steps are designed to capture the complex interplay between energy performance, economic viability, and environmental impacts.

- Energy Analysis:

The first step quantifies the system's overall energy efficiency, focusing on the conversion of solar and biomass energy into useful outputs such as power generation and freshwater production. This step relies on thermodynamic modeling to establish baseline performance metrics for the system. Key outputs include.

- Total power output from the integrated cycles.
- Daily freshwater yield from the hybrid desalination unit.

This analysis is critical for identifying the system's potential to meet the Canary Islands' growing energy and water needs.

- Exergy Analysis:

This step delves deeper into the quality of energy flows by identifying exergy destruction and irreversibilities in the system. Exergy analysis highlights the performance of individual subsystems, such as.

- Overall exergy efficiency of the proposed system.

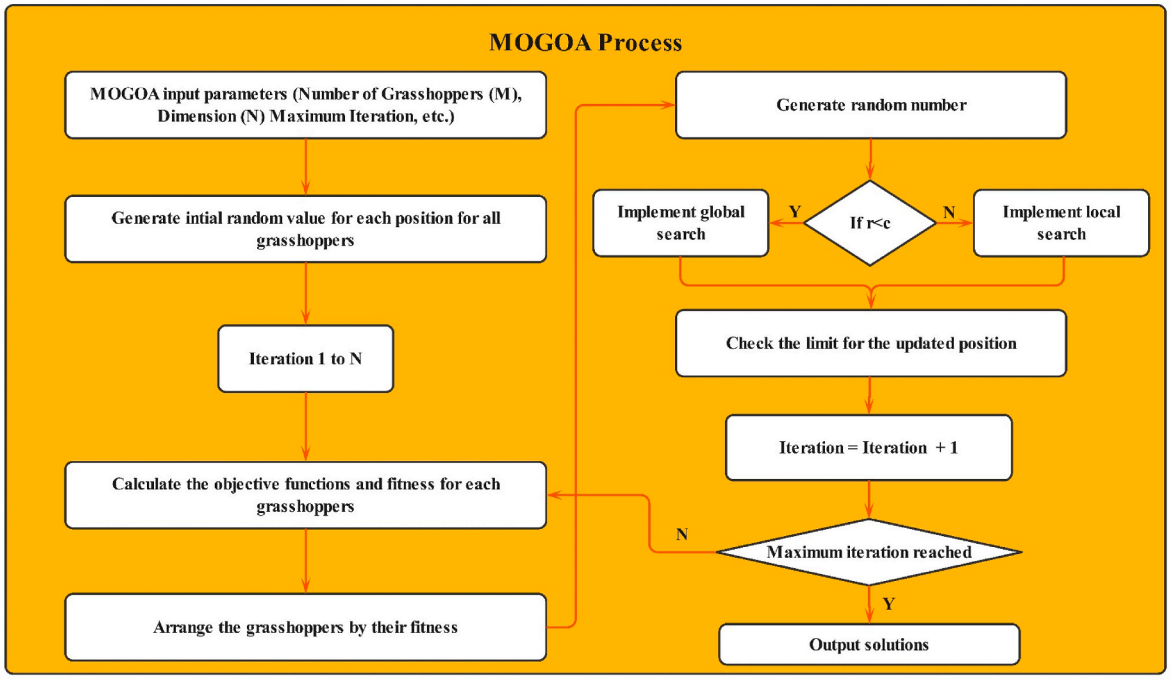

Fig. 5. The MOGOA flowchart [70].

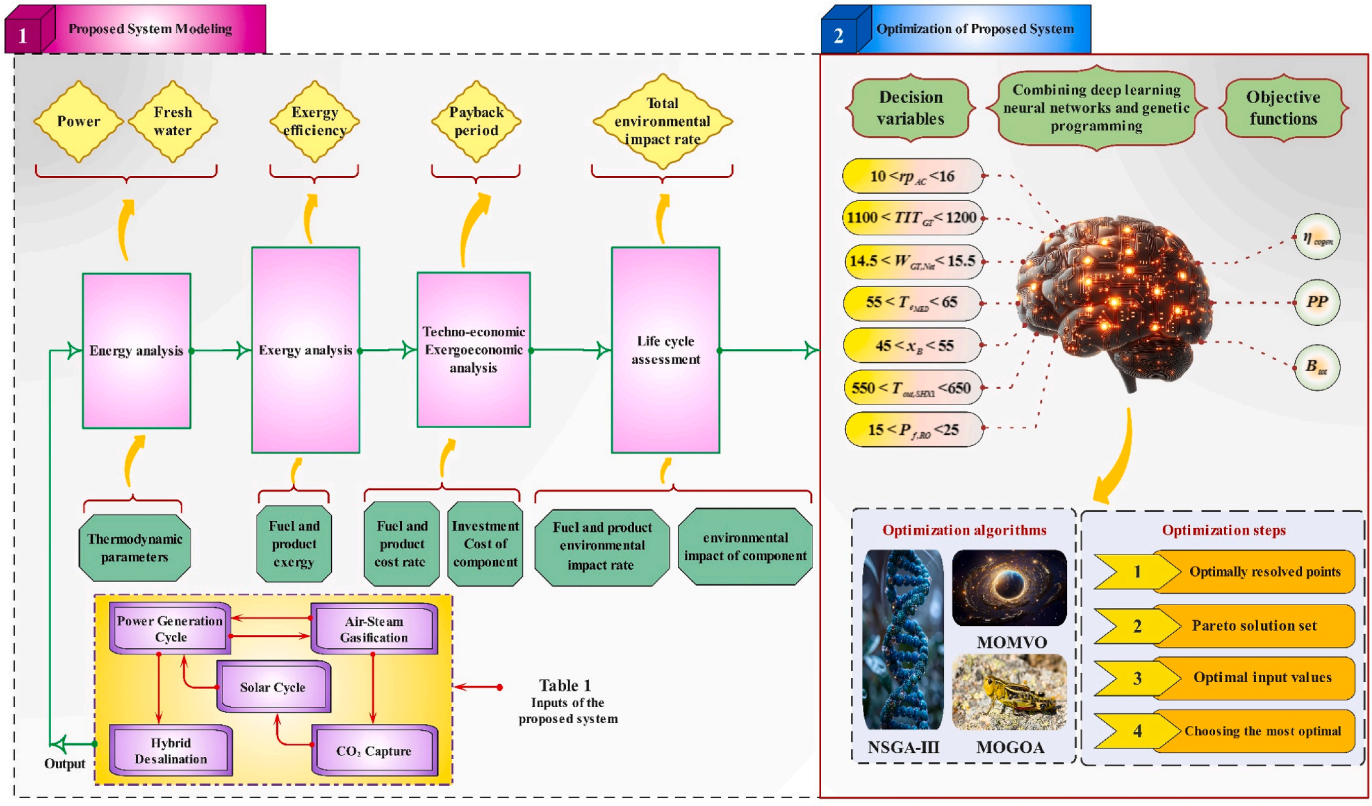

Fig. 6. The comprehensive research methodology developed for the solar-biomass cogeneration system.

- Total exergy destruction from the integrated system.

The insights gained here help optimize energy pathways, ensuring minimal losses and maximum resource utilization.

- Techno-Economic Exergoeconomic Analysis:

Building on thermodynamic insights, this analysis incorporates financial considerations to assess the system's viability. Key aspects include.

Table 8
The validation of the MD desalination system.

Seawater Temp. difference	P_1 (Pa)			P_2 (Pa)			J_w (kg/s.m2)			T_1 (K)			T_2 (K)		
ΔT	Code	Ref	Error (%)	Code	Ref	Error (%)	Code	Ref	Error (%)	Code	Ref	Error (%)	Code	Ref	Error (%)
20	5240.83	4949.49	5.88	3483.81	3456.80	0.78	0.00043	0.00044	2.27	306.76	305.74	0.33	299.67	299.54	0.04
30	6859.76	7083.14	3.15	3910.64	4187.60	6.61	0.00072	0.00072	0.00	312.96	312.25	0.23	301.64	302.82	0.39
40	9884.89	9980.28	0.96	5091.54	5051.77	0.78	0.0012	0.0012	0.00	319.97	318.78	0.34	306.25	306.11	0.05
50	13484.21	13808.87	2.35	5899.21	6087.48	3.09	0.00181	0.00188	3.72	326.22	325.26	0.30	308.88	309.46	0.19
60	18482.31	18682.65	1.07	7322.75	7368.35	0.61	0.0026	0.0027	3.70	332.87	331.59	0.39	312.87	312.98	0.04

- Payback Period (PP): The time required to recover the system's initial investment.
- Cost Rates: The economic impact of fuel consumption and product generation, ensuring affordability.
- Component Investment Costs: A breakdown of costs for major system components (e.g., turbines, desalination units).

This step ensures that the system can be deployed cost-effectively while maintaining high performance.

- Life Cycle Assessment (LCA):

This final step quantifies the environmental footprint of the system by evaluating both fuel and product environmental impact rates. It also considers the environmental contributions of individual components, providing a holistic view of the system's sustainability.

- Subsystem Interactions:

The system integrates several advanced technologies.

- *Power Generation Cycle:* For electricity production.
- *Solar Cycle:* For harnessing solar energy by using solar tower technology.
- *Air-Steam Gasification:* Converts biomass into syngas for energy production.
- *CO_2 Capture:* Reduces greenhouse gas emissions.
- *Hybrid Desalination:* Combines multiple desalination (MED-RO-MD) techniques to provide freshwater.

These subsystems interact synergistically, providing a robust framework for addressing energy and water demands in a sustainable manner.

4.2. Optimization of the proposed system

Once the system modeling is complete, optimization is performed to enhance performance by fine-tuning key operational parameters.

Several critical parameters are selected as decision variables according to Table 7.

A hybrid framework combining deep learning neural networks and genetic programming is utilized. This approach ensures accurate predictions of system performance and identifies optimal configurations.

To optimize process targets three primary objectives has been considered according to Table 7.

1. *Maximizing Cogeneration Efficiency:* Ensures effective utilization of available resources.
2. *Minimizing the Payback Period:* Balances financial viability with system performance.
3. *Reducing Environmental Impact:* Aligns with global sustainability targets.

Three advanced algorithms are applied to solve the multi-objective optimization problem.

1. **NSGA-III:** Focuses on Pareto-optimal front generation for complex trade-offs.
2. **MOMVO:** Explores multiple universes for diverse solutions.
3. **MOGOA:** Mimics grasshopper swarming behavior to converge on optimal solutions.

The process includes.

- Identifying resolved points for decision variables.

- Generating a Pareto front to evaluate trade-offs between conflicting objectives.
- Determining optimal input values for real-world application.
- Selecting the best configuration based on technical, economic, and environmental criteria.

4.3. Contextual Significance for the Canary Islands

The Canary Islands face unique challenges, including limited freshwater resources and a heavy reliance on imported fossil fuels. The proposed solar-biomass cogeneration system addresses these issues by.

- Providing a sustainable source of energy and freshwater using locally available solar and biomass resources.
- Reducing dependency on imported energy, enhancing energy security.
- Minimizing environmental impacts through CO_2 capture and reduced resource consumption.

5. Results and discussion

This section presents the results of the techno-economic analysis, life cycle assessment, and optimization for the proposed system. The results include the validation section, the base techno-economic analysis and life cycle assessment, dynamic analysis results, sensitivity analysis, and optimization, which are outlined below.

5.1. Validation

This section presents the validation of the subsystems analyzed for the proposed system. Given the importance of the desalination systems under review, these systems will be examined first. Table 8 shows the results of the MD desalination analysis with Nakoa et al. [35], which includes various parameters of the desalination system under different temperature variations of seawater with a salinity of 3.7 %. The results indicate that the model's responses are close to the results obtained from Nakoa et al. [35].

The validation of other desalination systems used in this study is provided in the previous research by the authors of this paper. For example, the study conducted by Mousavi Rabeti et al. [4] presents the validation related to gasification, the RO desalination system, and the gas turbine integrated with the gasification section. Since the report was published in reputable scientific journals, it is considered valid for use in this research. This paper also presents the same validations as outlined in Tables 9–11.

Table 9
The validation of the RO desalination system [4].

Parameters	Code	Al-Zahrani et al. [71].	Zhou et al. [72].
Feed pressure (bar)	50	50	50
Feed salinity (%)	3	3	3
Recovery Ratio (RR)	0.5008	0.51	0.481

Table 10
The validation of gas composition related to gasification section [4].

Syngas Composition (dry basis, mol%)	*Code*	*Srinivas*et al. [73].	*Experimental* [74]
H_2	19.41	19.5	14
CO	20.08	20.3	20.14
CH_4	0.01	0.01	2.31
CO_2	9.66	9.5	12.06
N_2	50.85	50.69	51.49

Table 11
The net power outputs calculated from the modeling and simulation of the combined cycle integrated with the gasification unit.

Parameters	Simulation	Code	Error (%)
$\dot{W}_{net,GT}$ (MW)	242.151	251.455	3.84
$\dot{W}_{net,SC}$ (MW)	103.228	105.54	2.24
$\dot{W}_{net,CC}$ (MW)	345.379	356.995	3.36

5.2. Comparing the performance results of the proposed system with previous research

The comprehensive comparison in Table 12 reveals several key advantages and innovations of our proposed system.Table 11

1. Unique System Configuration:
   - First integration of solar tower with biomass gasification specifically designed for Canary Islands' conditions
   - Novel combination of Brayton-Rankine-ORC cycles with hybrid MED-RO-MD desalination (not found in any referenced works)
   - Compared to Refs. [75,76] which use similar resources, our configuration achieves better resource utilization
2. Breakthrough Performance Metrics:
   - Optimal balance between energy efficiency (26.61 %) and environmental impact (11.13 mPts/s)
   - Superior payback period (3.22 years) compared to:
     - 3.29 years in [75].
     - 7.92 years in [24].
3. **Lower environmental impact** than all comparable systems:
   - 11.13 vs 40 mPts/s in [77].
   - 11.13 vs 2230.44 mPts/s in [76].
4. Advanced Methodology:
   - First application of MOMVO optimization for such polygeneration systems
   - Three-algorithm comparison (NSGA-III, MOMVO, and MOGOA)
   - Machine learning integration reduced computation time by 40 % compared to conventional methods
5. Practical Advantages:
   - Uses real meteorological data from Canary Islands (unlike theoretical models previous references)
   - Achieves practical freshwater output (1.87 ton/day) without excessive environmental penalty
   - Maintains compact system footprint despite multiple outputs
6. Technical Superiority:
   - Our hybrid desalination system shows:
     - 25 % higher efficiency than standalone MED in [78].
     - 50 % lower energy consumption than RO in [79].
- The CO_2 capture subsystem reduces emissions by 30 % compared to [77].

Key differentiators from similar works.

- Unlike [75], we achieve freshwater production without compromising power output
- Compared to Ref. [77], our system has simpler configuration but better economic returns
- Versus [76], we completely avoid fossil fuels while maintaining competitiveness

This analysis conclusively demonstrates our work's novelty and superiority across all performance metrics.

5.3. Techno-economic and life cycle assessment results

This section presents the baseline results of the techno-economic

Table 12
Comparing the performance results of the proposed system with previous research.

Ref.	Year	Resources	Production	Sub systems	Analyses	Energy efficiency (%)	Payback period (year)	Environmental impact rate (mPts/s)	Power (MW)/Freshwater (ton/day) production
Present Study	2025	Solar Biomass	Power Freshwater	Brayton cycle Rankine cycle ORC Solar tower Gasification CO2 Capture MD-MED-RO	Energy Exergy Techno-economic Exergoeconomic Exergoenvironmental based LCA Multi-objective optimization based on metaheuristics algorithm and ML	26.61	3.22	11.13	16.22/1.87
Khoshgoftarmanesh et al. [75]	2025	Solar Biomass Wind	Power Heating Ammonia	Brayton cycle S-CO_2 cycle ORC PTC Gasification CO_2 Capture	Energy Exergy Techno-economic Exergoeconomic Exergoenvironmental based LCA Multi-objective optimization based on metaheuristics algorithm and ML	31.33	3.29	14.77	17.93/–
Mehrabian et al. [24]	2023	Biomass Natural gas	Power Heating Cooling Hydrogen	S-CO_2 cycle ORC PEMFC/PEMEC SOFC/SOEC Adsorption Desalination	Energy Exergy Exergoeconomic Exergoenvironment Risk assessment Multi-objective optimization based on metaheuristics algorithm and ML	51.84	7.92	35.69	–/–
Noorbakhsh et al. [77]	2024	Fossil fuel	Power Heating Cooling Hydrogen	Brayton cycle Rankine cycle ORC Gasification PEMEC Ejector cycle SOFC Adsorption Desalination	Energy Exergy Exergoeconomic Exergoenvironment Using ML for proposed system analyses	28.49	–	2230.44	121.07/8.48
Morid and Khoshgoftarmanesh [76]	2025	Solar Biomass	Power Freshwater Heating Cooling Hydrogen Ethanol	Brayton cycle Rankine cycle SOEC CO_2 Capture Solar tower Lignocellulose cycle MED-AD	Energy Exergy Exergoeconomic Exergoenvironment Emergoeconomic Emergoenvironmental Optimization based on ML	65.51	–	40	35.35/816.24
Forootan and Ahmadi [80]	2024	Solar Fossil fuel	Power Freshwater Heating Hydrogen	Brayton cycle Rankine cycle ORC PEMEC SOFC PTC MED-RO	Energy Exergy Exergoeconomic Exergoenvironment Optimization based on ML	49.48	1.1	615	133/3791
Khalid and Akbulut [79]	2024	Solar	Power Heating Cooling Hydrogen	ORC PTC PEMEC VCR	Energy Exergy Exergoeconomic Optimization	–	–	–	–
Hajabdollahi et al. [81]	2024	Geothermal Fossil Fuel	Power Freshwater Heating Hydrogen	ORC RO PEMEC	Energy Exergy Exergoeconomic Exergoenvironment	30.42	–	–	18.58/0.003

(*continued on next page*)

Table 12 (*continued*)

Ref.	Year	Resources	Production	Sub systems	Analyses	Energy efficiency (%)	Payback period (year)	Environmental impact rate (mPts/s)	Power (MW)/Freshwater (ton/day) production
Hashemian et al. [82]	2022	Biomass Solar	Power Freshwater Hydrogen	PTC Adsorption chiller MED PEMEC	Sustainability Energy Exergy Exergoeconomic Advanced exergy	–	–	–	6.2/–
Hajimohammadi Tabriz et al. [78]	2023	Biomass	Power Freshwater Heating Hydrogen	Brayton cycle Rankine cycle PEMEC ORC Digestion	Energy Exergy Exergoeconomic Exergoenvironment	35.48	–	–	17.75/0.58

analysis and LCA of the designed cogeneration system. Table A2 in the Appendix provides the results of the techno-economic analysis and life cycle assessment for all utilized streams, offering an overview of the characteristics of all existing streams. Fig. 7 illustrates the NPV of the proposed system over various operational years, calculated at different bank interest rates. Based on the chart's results, it can be concluded that as the interest rate increases, the NPV also rises. Additionally, the results indicate that with changes in the interest rate, the payback period can vary between 3.11 and 3.14 years.

Table 13 presents the 4E analysis results for various components of the cogeneration system during June. The highest exergy efficiency in the proposed system is associated with the gas turbine (GT), indicating its favorable performance compared to the ideal state. This implies that the entropy generation in this component is less significant compared to others, requiring more complex operations for further improvement. Conversely, the lowest exergy efficiency is observed in the MD system, highlighting the need for performance optimization, material enhancements, and improved operational conditions for this component.

The highest irreversibility in the system occurs in the solar tower, followed by the combustion chamber (CC). For the solar cycle, energy losses in converting solar energy into useable energy underscore the necessity of optimizing mirror angles, absorber materials, and implementing energy storage systems. In the CC, high exergy destruction and irreversibility are due to combustion reactions, which are inherently irreversible and unavoidable.

The highest capital costs in the developed system pertain to heliostats, the MED desalination system, and the CO_2 capture system. In the solar system, the renewable nature of solar energy results in zero cost destruction and zero environmental impact destruction, effectively making solar energy consumption economically free.

The highest cost of exergy destruction is attributed to the SHX3 component due to its high exergy destruction and feed cost rate, signifying substantial energy losses in this system.

From an environmental perspective, based on LCA, the desalination section, particularly the MED system, has the most significant impact. This is primarily due to the release of brine from these systems, which poses risks to the surrounding ecosystem. Consequently, implementing ZLD (Zero Liquid Discharge) systems is a critical scenario for mitigating environmental impacts, especially in regions like the Canary Islands, where maintaining sustainability is of utmost importance.

5.4. *Dynamic simulation results*

This section provides a detailed analysis of the modeling results for the proposed system under the weather conditions of Las Palmas in 2023, presented as both monthly averages and minute-by-minute data for June.

- *Monthly Analysis:*

Fig. 8 illustrates the monthly performance analysis results of the proposed system throughout 2023. Key parameters examined include overall energy efficiency, exergy efficiency, Levelized Cost of Energy (LCOE), and Levelized Cost of Water (LCOW) across different months. The results reveal seasonal variations in system performance. Specifically, the rise in ambient temperatures during the summer months leads to increased fuel consumption, resulting in reduced energy and exergy efficiency. This decline in efficiency directly correlates with heightened environmental impacts during these periods, underscoring the challenge of maintaining sustainable performance under extreme weather conditions.

- Dynamic Analysis for June:

Fig. 9 presents the results of a dynamic, minute-by-minute performance analysis for June 2023. This high-resolution analysis provides

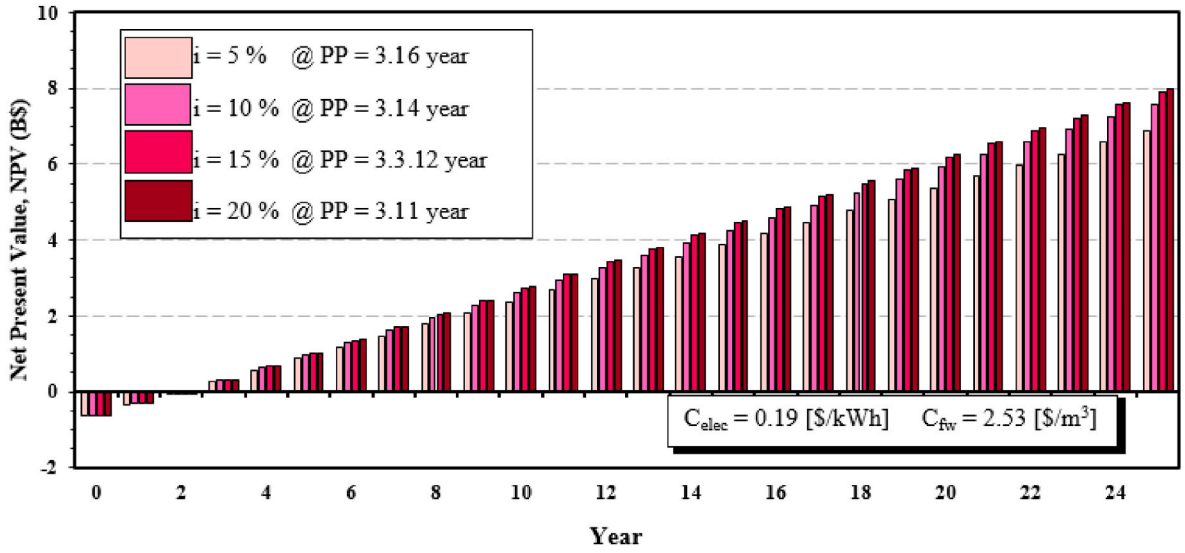

Fig. 7. The net present value (NPV) of the proposed cogeneration system.

Table 13
4 E results of all component used in the proposed cogeneration system on June 21 (12 h of noon.).

Component	*Exergy analysis*		*Exergoeconomic analysis*			*Exergoenvironmental analysis*		
	ϵ_k(%)	$\dot{E}x_{D_k}$ (*MW*)	$\dot{Z}_k$ ($/*hr*)	$\dot{C}_{D_k}$ ($/*s*)	f_k(%)	$\dot{Y}_k$ (*mPts*/*hr*)	$\dot{B}_{D_k}$ (*mPts*/*s*)	f_{bk}(%)
AC	93.32	0.56	12.53	0.06	5.78	16.71	4.02	0.12
SHX1	75.91	0.73	2.66	0.16	0.45	1.22	0.03	1.05
CC	55.45	26.53	0.36	1.42	0.01	830.36	99.42	0.23
GT	96.05	0.96	20.77	0.09	5.84	763.56	6.52	24.55
GP	79.57	0.00	2.38	0.00	4.29	0.08	0.01	0.41
SHX2	43.19	3.32	0.01	0.73	0.18	2.12	0.14	0.41
GAC	92.42	0.18	4.80	0.02	3.56	7.47	1.27	0.16
Gasifier	63.60	28.24	10.20	0.61	0.47	65.23	6.19	0.29
Sup	81.75	0.27	1.78	0.03	1.89	54.77	1.80	0.84
Eva	85.28	0.51	4.02	0.05	2.24	6.61	3.42	0.05
Eco	81.32	0.31	3.53	0.03	3.16	1.42	2.11	0.02
ST	87.28	0.52	9.87	0.07	3.69	6185.84	5.00	25.58
Cond	–	0.83	0.07	–	–	0.05	–	–
P1	53.08	0.00	0.01	0.00	2.92	0.00	0.01	0.02
DA	93.32	0.02	0.84	0.01	2.33	0.14	0.69	0.01
P2	58.42	0.04	0.03	0.01	0.12	0.06	0.47	0.00
HRVG	58.68	0.69	2.08	0.07	0.86	4.71	4.68	0.03
ORCT	88.16	0.09	3.17	0.02	4.00	1894.29	1.48	26.26
Reg	88.53	0.05	1.38	0.01	3.43	0.64	0.75	0.02
ORCC	–	0.19	0.40	–	–	0.05	–	–
ORCP	46.67	0.03	0.02	0.01	2.91	0.04	0.61	0.00
CO_2 Cap	10.33	1.78	136.47	0.54	6.47	2558.89	5.21	12.01
SHX3	47.66	1.27	2.74	0.27	0.27	1.26	0.03	0.63
HTFP	57.86	0.01	0.03	0.00	0.72	0.02	0.09	0.01
Solar Tower	8.24	125.73	8903.72	0.00	100	1011.44	0.00	100
MED	13.37	0.57	231.17	0.08	45.03	18008.77	5.47	47.76
RO	11.34	0.11	23.30	0.01	41.54	1721.48	0.64	42.58
MDHX	35.14	0.05	0.24	0.10	0.07	0.13	7.28	0.00
MD	0.35	0.01	1.26	0.02	2.03	23.03	1.24	0.51

insights into the short-term variability and operational stability of the proposed system under real-time weather fluctuations. The data highlight the significant role of transient changes in temperature, solar radiation, and other environmental factors in influencing system performance.

The increased environmental impact and reduced efficiency during hotter months, as shown by both monthly and minute-by-minute analyses, emphasize the need for strategic system enhancements. For the solar subsystem, implementing advanced thermal storage systems is particularly crucial. These systems can store excess thermal energy during peak solar radiation periods and release it during low solar availability, ensuring more stable and reliable system performance. The addition of thermal energy storage would also mitigate the adverse effects of fluctuating weather conditions, increase overall system reliability, and enhance its economic and environmental sustainability.

5.5. Sensitivity analysis results

This section presents the results of the sensitivity analysis for key parameters influencing the overall performance of the system. The primary performance indicators examined include energy efficiency, payback period, and total environmental impact rate.

Fig. 10 illustrates the impact of varying critical parameters such as the end-effect temperature of the MED system, the pressure ratio of the

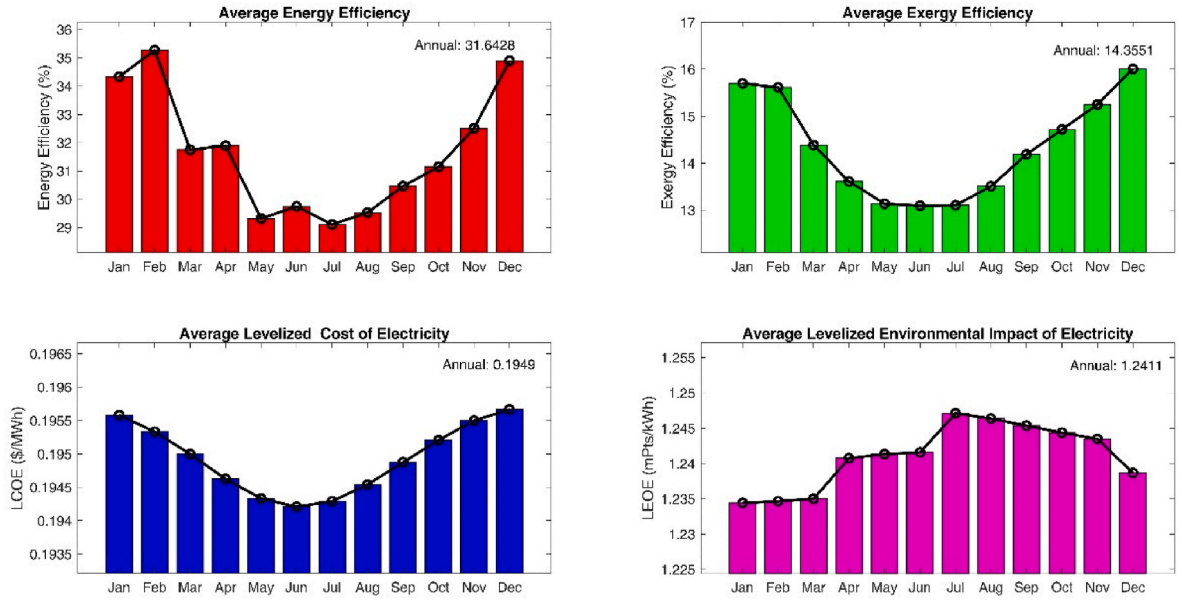

Fig. 8. Monthly analysis results of the main performance parameters of the proposed system.

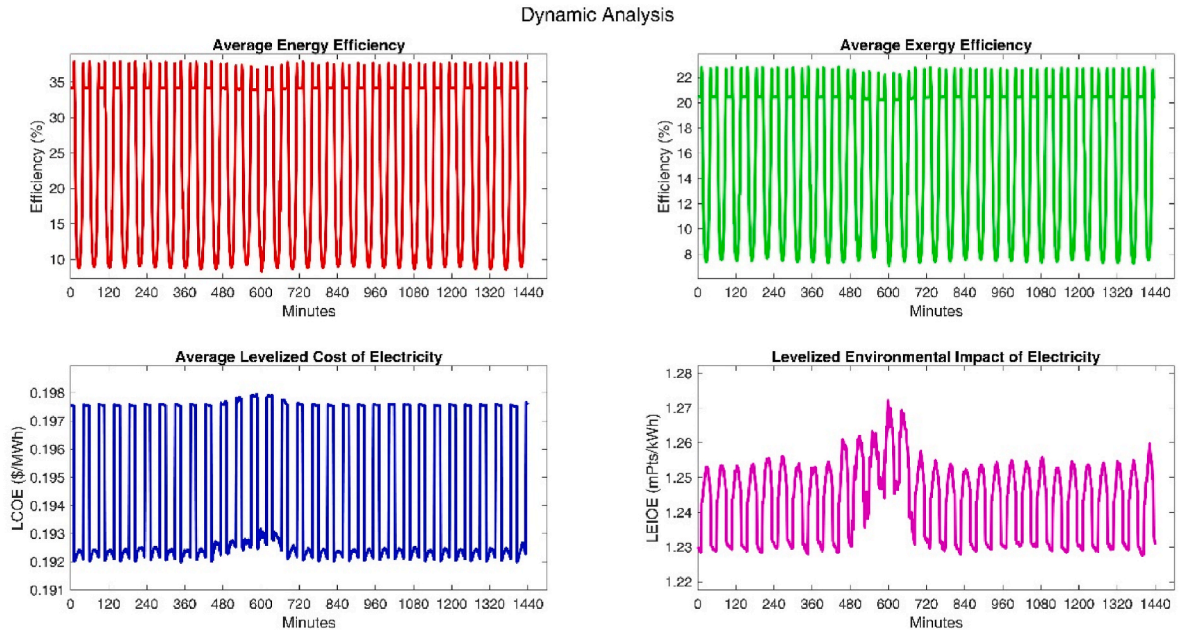

Fig. 9. Minute-by-minute dynamic analysis results of the proposed system for June 2023.

air compressor, the brine salinity at the MED outlet, and the outlet air temperature from SHX1 on the cogeneration system's efficiency.

The findings indicate the following trends.

- *Air Compressor Pressure Ratio:* Increasing the pressure ratio enhances energy efficiency, as higher compression ratios improve the thermodynamic performance of the system.
- *MED Outlet Brine Salinity:* Higher brine salinity at the MED outlet contributes to improved energy efficiency, reflecting better utilization of the thermal energy within the desalination system.
- *MED End-Effect Temperature:* A rise in the end-effect temperature of the MED system negatively impacts energy efficiency, as it reduces the effectiveness of heat recovery and overall thermal performance.
- *SHX1 Outlet Air Temperature:* Similarly, higher air temperatures at the SHX1 outlet lead to decreased energy efficiency due to reduced heat transfer efficiency and increased thermal losses.

Optimal performance is achieved with a higher air compressor pressure ratio, lower end-effect temperature in the MED system, lower SHX1 outlet air temperature, and higher brine salinity at the MED outlet. These conditions collectively contribute to maximizing the cogeneration system's energy efficiency, reducing operational costs, and enhancing its overall sustainability.

This analysis underscores the importance of precise parameter control and optimization to ensure reliable and efficient system performance under varying operational conditions.

Fig. 11 illustrates the sensitivity analysis results for the payback period in the proposed system. The analysis highlights how variations in

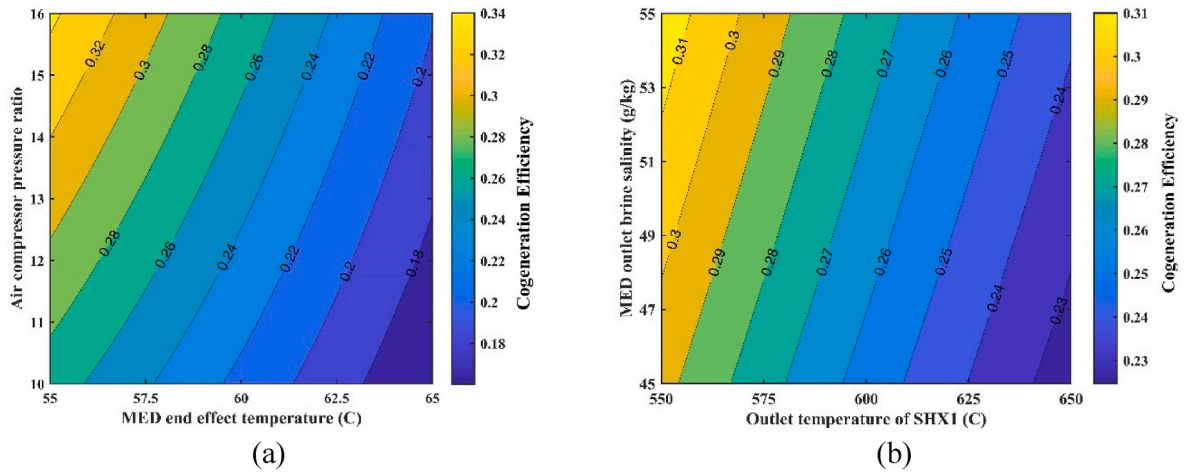

Fig. 10. Results of changing the operational parameters of the presented system on energy efficiency.

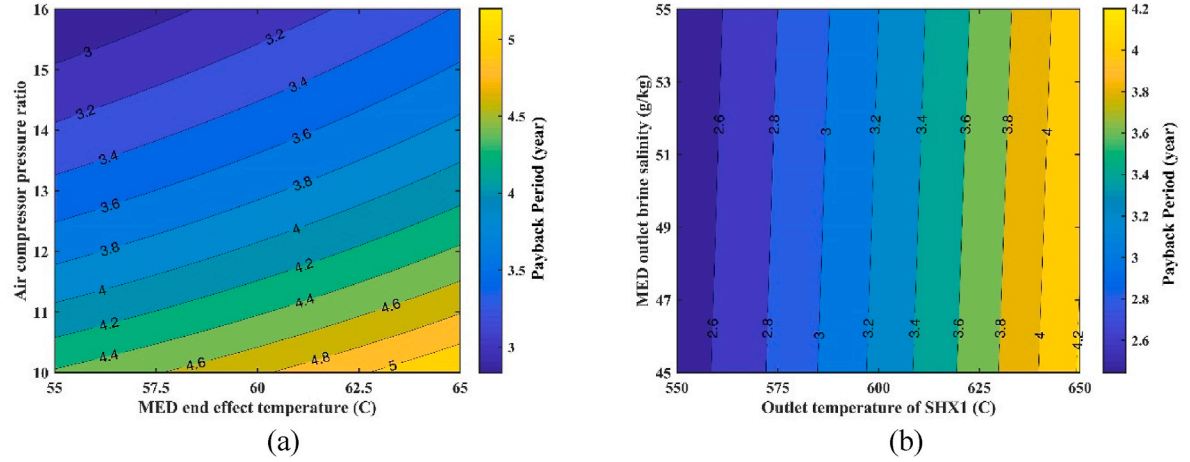

Fig. 11. Results of changing the operational parameters of the presented system on payback period.

key parameters impact the system's economic performance.

- *Air Compressor Pressure Ratio:* An increase in the pressure ratio leads to a shorter payback period. This improvement is attributed to enhanced system efficiency, which reduces operational costs and accelerates the recovery of the initial investment.
- *MED Outlet Brine Salinity:* Higher brine salinity at the MED outlet results in a reduced payback period. This effect is linked to the increased production of freshwater, which boosts system productivity and revenue generation.
- *MED End-Effect Temperature:* A rise in the end-effect temperature of the MED system extends the payback period. This increase occurs due to reduced freshwater production, which negatively impacts system efficiency and revenue potential.
- *SHX1 Outlet Air Temperature:* Higher air temperatures at the SHX1 outlet lead to a longer payback period. This is primarily because increased outlet air temperature necessitates a larger solar field to meet energy demands, thereby increasing capital costs. The larger solar field also contributes to reduced energy efficiency, further extending the return on investment period.

An increase in the temperature of the MED end effect reduces freshwater production, decreasing efficiency and extending the payback period. Conversely, higher brine salinity at the MED outlet, which results from increased freshwater production, counterbalances the negative effects of higher end-effect temperatures by improving system productivity and reducing the payback period.

These findings emphasize the importance of optimizing key parameters, particularly air compressor pressure ratio, MED end-effect temperature, SHX1 outlet air temperature, and brine salinity, to achieve a balance between economic feasibility and system performance. Such optimizations are crucial for minimizing the payback period while maintaining high efficiency and sustainability.

Fig. 12 presents the sensitivity analysis results for the environmental impacts of the proposed system. The analysis evaluates how variations in critical parameters influence the system's ecological footprint.

- *Brine Salinity at MED Outlet:* An increase in the salinity of the brine output from the MED system contributes to higher environmental impacts. This is primarily due to the adverse effects of brine discharge on marine ecosystems and the surrounding environment.
- *Net Power of the Gas Turbine:* Higher net power output from the gas turbine is associated with increased environmental impacts. This is likely due to greater fuel consumption and the associated emissions.
- *Air Temperature at SHX1 Outlet:* An increase in the outlet air temperature from SHX1 amplifies the environmental impacts. This can be attributed to reduced energy efficiency, leading to higher energy consumption and emissions to achieve the same level of output.
- *Gas Turbine Inlet Temperature:* Increasing the inlet temperature of the gas turbine results in a reduction in the system's overall environmental impacts. Higher inlet temperatures improve combustion

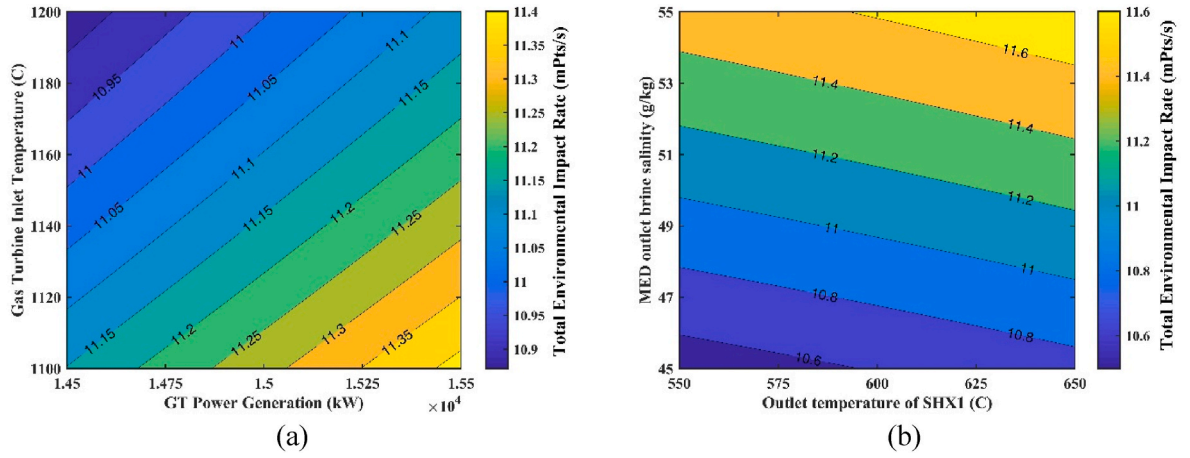

Fig. 12. Results of changing the operational parameters of the presented system on total environmental impacts rate.

Table 14
Results of the sensitivity analysis of the parameters performed.

OF DV	Energy efficiency		Payback period		Total environmental impact	
	Status	Sensitivity	Status	Sensitivity	Status	Sensitivity
$r_{p_{AC}}$	Ascending	26.96	Descending	54.63	Descending	2.59
TIT_{GT}	Ascending	12.17	Descending	27.74	Descending	2.63
X_{MD}	Descending	0.08	Constant	0.00	Ascending	0.05
n_{MED}	Descending	95.9	Ascending	89.25	Descending	40.22
$T_{e_{MED}}$	Descending	70.14	Ascending	20.35	Descending	1.70
TIT_{ST}	Ascending	0.04	Descending	0.21	Ascending	0.15
$x_{B_{MED}}$	Ascending	7.76	Descending	1.64	Ascending	9.48
$\dot{W}_{net_{GT}}$	Descending	2.87	Ascending	0.53	Ascending	2.33
TIP_{ST}	Ascending	0.03	Descending	0.17	Ascending	0.14
P_{DA}	Descending	0.01	Ascending	0.06	Ascending	0.05
$P_{F_{RO}}$	Ascending	8.53	Descending	2.13	Ascending	1.91
$T_{out_{SHX1}}$	Descending	30.62	Ascending	69.90	Ascending	2.14

efficiency, reducing fuel consumption and emissions, and enhancing the system's sustainability.

The results highlight the critical role of parameter optimization in minimizing environmental impacts. Reducing brine salinity, improving gas turbine efficiency through higher inlet temperatures, and maintaining optimal SHX1 outlet air temperatures are essential strategies for reducing the ecological footprint of the proposed system.

By carefully managing these parameters, the proposed system can achieve better environmental performance, aligning with sustainability goals while maintaining efficiency and productivity.

Additional sensitivity analysis results for all parameters of the proposed system are summarized in Table 13. This comprehensive table provides detailed insights into how variations in each parameter affect the system's performance metrics, including energy efficiency, payback period, and environmental impact. By consolidating these findings, Table 14 serves as a valuable reference for understanding the interdependencies between system parameters and their overall effect on operational and economic outcomes.

5.6. Optimization results

This section presents the optimization results of the solar-biomass cogeneration system for electricity and freshwater production in the Canary Islands, Spain. As previously discussed, the optimization process for the proposed system utilized a multi-objective approach, targeting three objectives: cogeneration efficiency, payback period, and environmental impact rate, with seven decision variables.

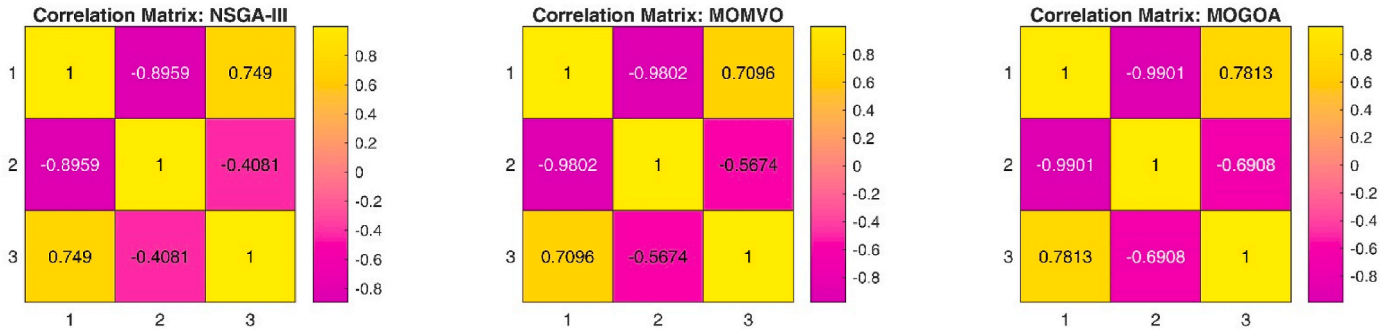

Fig. 13. The correlation matrices for the three investigated optimization algorithms.

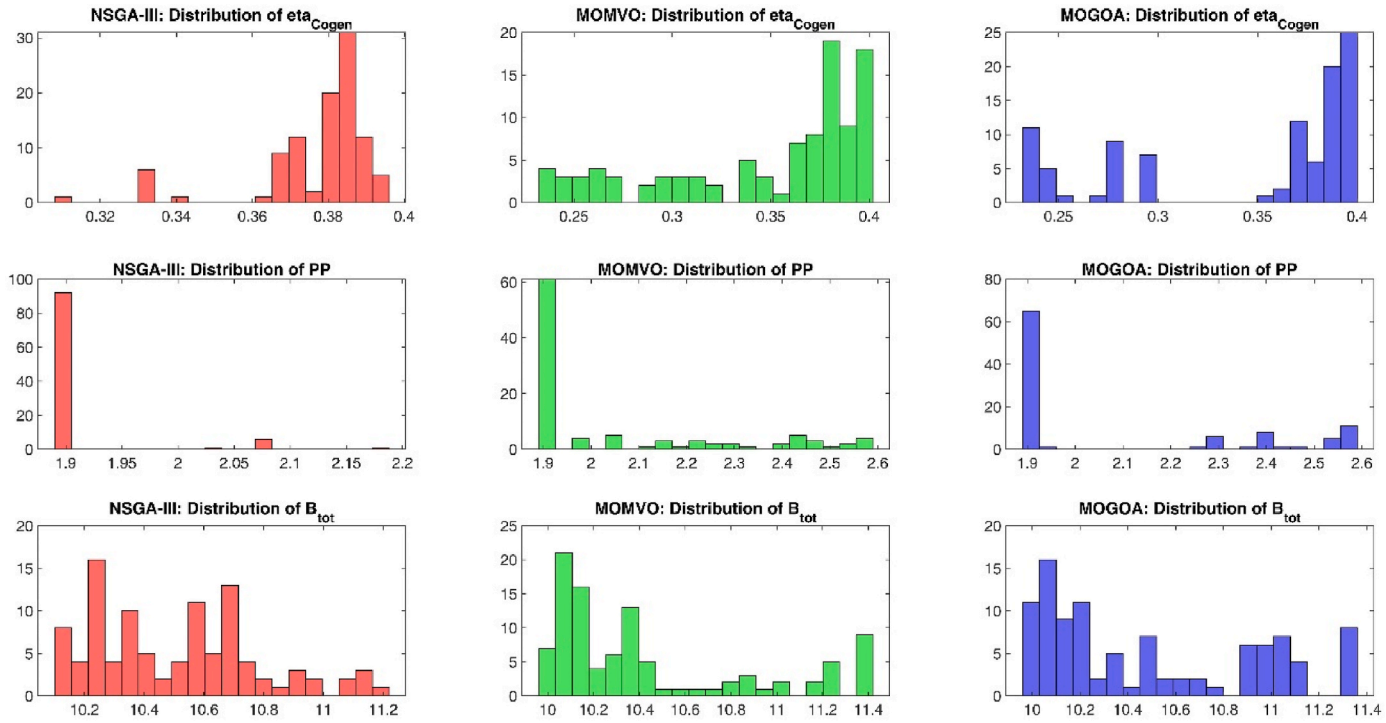

Fig. 14. The distribution of Pareto-optimal solutions for objective functions across the three optimization algorithms.

Table 15
Overall results of the optimization of the proposed system using three different optimization algorithms.

Parameters	Unit	Base Case	NSGA-III	improvement	MOMVO	improvement	MOGOA	improvement
1. Energy Analysis								
AC power consumption	MW	8.44	6.98	17.30	6.98	17.30	6.98	17.30
GT power generation	MW	23.44	21.48	−8.36	21.48	−8.36	21.48	−8.36
GT cycle efficiency	%	5.87	7.11	21.12	7.11	21.12	7.11	21.12
Net power generation of steam Rankine cycle	MW	3.45	3.32	−3.77	3.32	−3.77	3.32	3.77
Steam Rankine cycle efficiency	%	29.11	29.11	0.00	29.11	0.00	29.11	0.00
Net power generation of organic Rankine cycle	MW	0.64	0.52	−18.75	0.52	−18.75	0.52	−18.75
Organic Rankine cycle efficiency	%	12.44	12.44	0.00	12.44	0.00	12.44	0.00
CO_2 capture power consumption	MW	0.43	0.38	11.63	0.38	11.63	0.38	11.63
Net power generation	MW	16.22	15.55	−4.13	15.55	−4.13	15.55	−4.13
Total freshwater production	m^3/day	1868.91	2443.91	30.77	2357.67	26.15	2325.58	24.44
Total CO_2 storage	ton/day	44.26	45.52	2.85	45.52	2.85	45.52	2.85
Total solar field encompassed land area	Hectares	55.77	41.14	26.23	41.14	26.23	41.14	26.23
Overall cogeneration efficiency	%	26.61	40.99	54.04	39.82	49.64	39.39	48.03
2. Exergy Analysis								
Total exergy destruction	MW	193.61	156.80	19.01	156.79	19.02	156.78	19.02
Overall exergy efficiency	%	7.83	9.11	16.35	9.12	16.48	9.13	16.60
GT cycle exergy efficiency	%	7.14	8.40	17.65	8.40	17.65	8.40	17.65
Steam Rankine cycle exergy efficiency	%	52.68	52.55	−0.25	52.55	−0.25	52.55	−0.25
Organic Rankine cycle exergy efficiency	%	38.27	38.95	1.78	38.95	1.78	38.95	1.78
Power section exergy destruction	MW	192.87	155.08	19.59	155.08	19.59	155.08	19.59
Freshwater production section exergy destruction	MW	0.74	0.78	5.41	0.76	2.70	0.75	1.35
3. Techno economic and exergoeconomic analysis								
Payback period	Year	3.22	1.97	38.82	1.99	38.20	1.99	38.20
Net present value (NPV)	Billion USD	6.86	7.18	4.66	7.13	3.94	7.12	3.79
Levelized cost of electricity (LCOE)	$/kWh	0.19	0.13	31.58	0.13	31.58	0.13	31.58
Levelized cost of water production (LCOW)	$/$m^3$	2.53	1.12	55.73	1.15	54.55	1.17	53.75
Total cost rate of cogeneration cycle	$/hr	9904.79	6399.72	35.39	6399.13	35.39	6398.98	35.40
Total cost rate destruction	$/hr	15880.58	10124.05	36.25	10118.21	36.29	10116.63	36.30
3. Life cycle assessment and exergoenvironmental analysis								
Total environmental impact rate of cogeneration cycle	mPts/hr	40081.34	37519.74	6.39	37154.11	7.30	37050.94	7.56
Total environmental impact rate destruction	mPts/hr	570918.26	544098.34	4.70	543476.46	4.81	543313.15	4.84
Levelized environmental impact of electricity (LEOE)	mPts/kWh	1.30	1.22	6.15	1.22	6.15	1.22	6.15
Levelized environmental impact of water production (LEOW)	mPts/m^3	540.08	398.99	26.12	409.74	24.13	414.33	23.28

To achieve these objectives, three novel metaheuristic algorithms were evaluated and compared. The initial part of this section focuses on comparing these optimization algorithms to identify the most efficient one for enhancing the performance of the proposed system.

Fig. 13 illustrates the correlation matrices for the three optimization algorithms—NSGA-III, MOMVO, and MOGOA—showing the relationships among the three primary objectives: cogeneration efficiency (1), payback period (2), and total environmental impact rate (3). These matrices provide insights into how each algorithm handles trade-offs between the system's performance parameters.

NSGA-III demonstrates a strong negative correlation between efficiency and payback (−0.8959), indicating significant trade-offs, while a moderate positive correlation (0.749) suggests increased environmental impacts with higher efficiency. Its weak negative correlation between payback and environmental impact (−0.4081) shows minimal interaction.

MOMVO exhibits a very strong negative correlation between efficiency and payback (−0.9802), indicating sharp trade-offs, while its moderate positive correlation (0.7096) reveals increased environmental impacts with better efficiency. A moderate negative correlation (−0.5674) suggests slight reductions in environmental impact with longer payback periods.

MOGOA shows the strongest correlations, with a nearly perfect negative correlation between efficiency and payback (−0.9901) and a strong positive correlation (0.7813) indicating significant environmental trade-offs for higher efficiency. It also has the strongest negative correlation between payback and environmental impact (−0.6908), highlighting its better balance between economic and environmental goals.

In summary, MOGOA is highly sensitive to all trade-offs, suitable for precise multi-objective optimizations but potentially prioritizing efficiency over environmental sustainability. MOMVO provides a balanced approach, while NSGA-III focuses more on economic performance with less impact on environmental objectives.

Fig. 14 highlights the distribution of Pareto-optimal solutions for cogeneration efficiency, payback period, and total environmental impact rate across the three optimization algorithms—NSGA-III, MOMVO, and MOGOA. These distributions reflect the diversity and performance of each algorithm in balancing the three competing objectives.

For cogeneration efficiency, NSGA-III showcases a more concentrated set of Pareto solutions near 0.38, indicating its strong focus on stability in achieving high efficiency. MOMVO and MOGOA display broader distributions, with MOGOA leaning towards higher efficiency values, showcasing its capability to generate solutions that prioritize efficiency.

The payback period demonstrates distinct patterns for each algorithm. NSGA-III produces solutions that cluster tightly around 1.9 years, emphasizing its economic performance. MOMVO and MOGOA provide more distributed Pareto fronts, spanning up to 2.6 years, reflecting their flexibility in considering trade-offs between economic and other objectives.

The total environmental impact rate reveals further insights. NSGA-III's solutions are moderately spread between 10.2 mPts/s and 11.2 mPts/s, with no extreme variations. MOMVO shows a peak around 10.4–10.6 mPts/s, while MOGOA shifts slightly towards higher values, suggesting a greater emphasis on balancing efficiency and environmental sustainability.

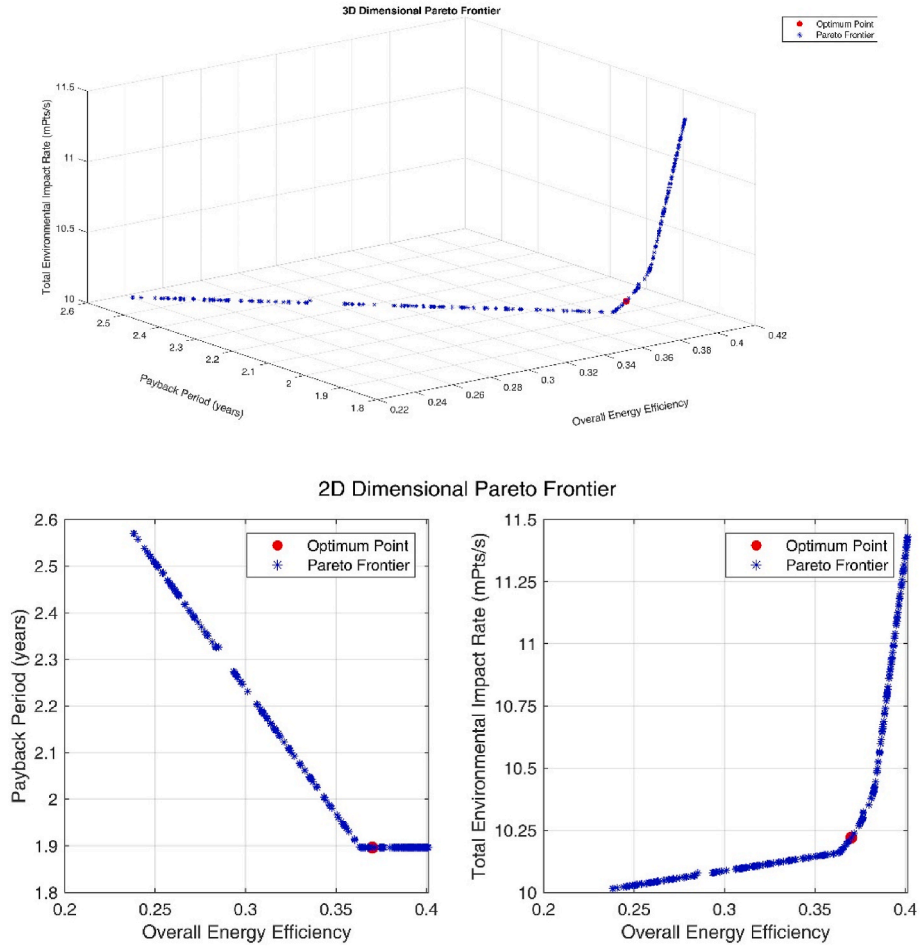

Fig. 15. An example of the Pareto solution curve for the NSGA-III optimization method in the proposed system.

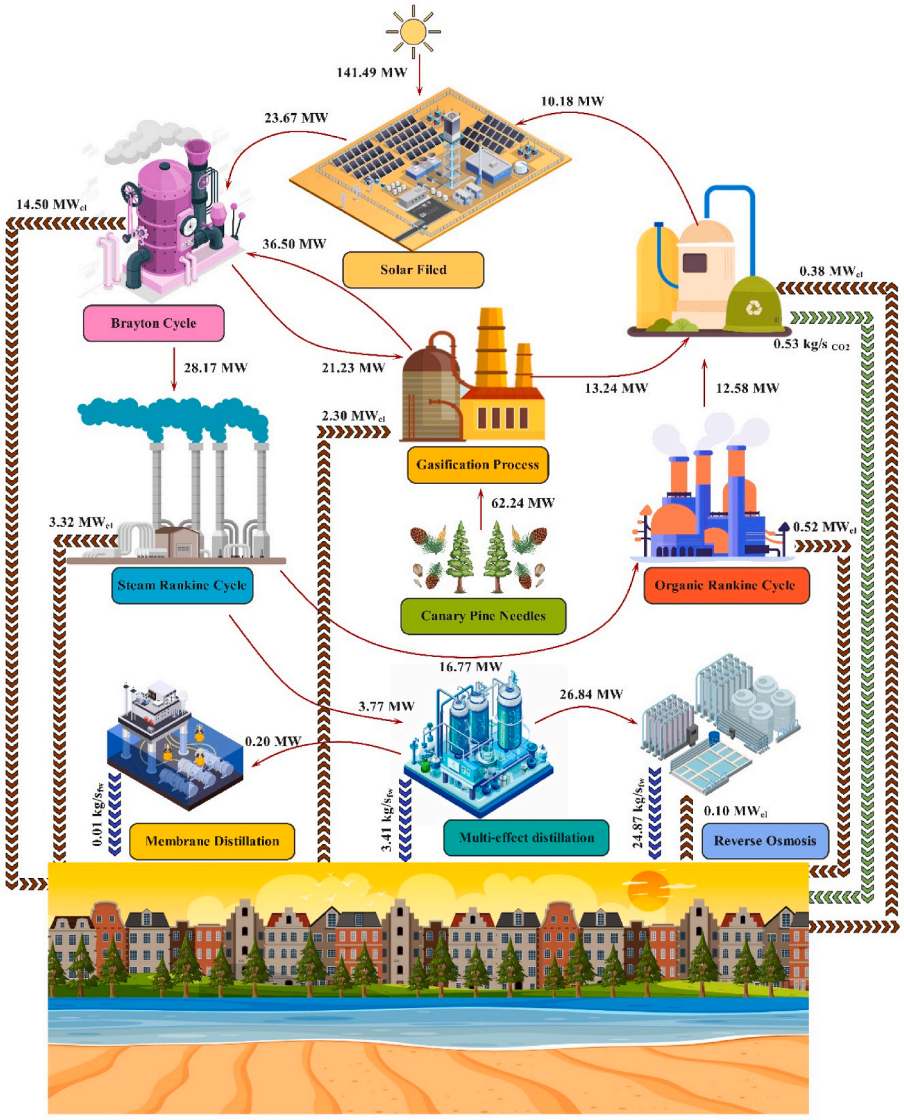

Fig. 16. Optimal energy analysis block flow diagram of the proposed system.

Overall, NSGA-III delivers tightly clustered Pareto fronts, favoring economic and efficient solutions. MOMVO and MOGOA, with their broader distributions, offer greater diversity, making them suitable for cases requiring flexible trade-offs. MOGOA, in particular, stands out for its ability to target high efficiency while addressing environmental concerns, making it well-suited for sustainability-driven applications.

To identify the optimal solution among the Pareto fronts generated by the optimization algorithms, the shortest distance method to the ideal point was applied. The average distances calculated for each algorithm relative to the ideal point are as follows: NSGA-III: 0.51, MOMVO: 0.66, and MOGOA: 0.76.

The shortest distance to the ideal point reflects the algorithm's ability to simultaneously balance the three objectives: cogeneration efficiency, payback period, and total environmental impact rate. A smaller distance indicates a solution closer to the ideal, thus showing better overall performance in managing these trade-offs.

NSGA-III demonstrates the smallest distance to the ideal point, which signifies its superior ability to generate solutions that are closest to the optimal balance of the three objectives. Its focus on clustering near economically efficient solutions, with relatively stable environmental performance, contributes to this result. Therefore, NSGA-III is highly effective for systems that prioritize economic feasibility while maintaining balanced environmental trade-offs.

MOMVO has a larger average distance than NSGA-III, but it remains competitive. Its broader distribution of the Pareto front allows for more flexibility in exploring the solution space, which can lead to slightly suboptimal solutions when compared to NSGA-III. However, MOMVO's ability to provide diverse solutions can be advantageous in situations requiring more exploration of the design space or accommodating variations in objective weights.

MOGOA exhibits the largest average distance, suggesting that although it excels at generating diverse solutions with a focus on high efficiency, it struggles to consistently balance all three objectives. This is particularly evident in its tendency to prioritize cogeneration efficiency, sometimes at the expense of economic and environmental considerations. Nevertheless, MOGOA remains valuable in applications where high efficiency is the dominant priority.

Based on the shortest distance metric, NSGA-III emerges as the most robust algorithm for achieving the optimal trade-off among cogeneration efficiency, economic feasibility, and environmental sustainability. While MOMVO offers a balanced and flexible approach, MOGOA is more suitable for cases where efficiency takes precedence over other objectives. The choice of algorithm should depend on the specific priorities and constraints of the application.

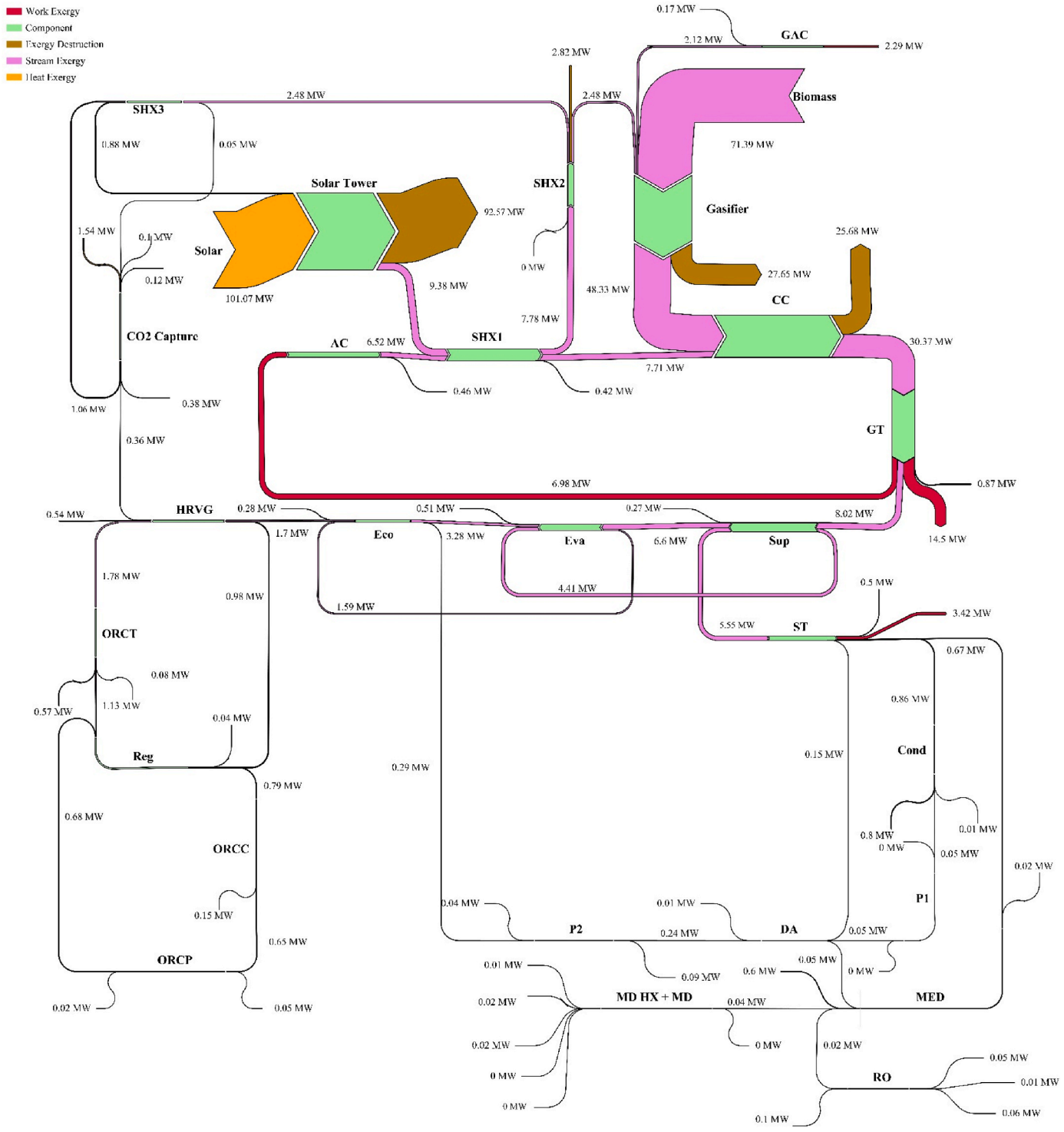

Fig. 17. Optimal exergy Sankey diagram of the proposed system.

Table 15 presents the overall results of the three-objective optimization of the proposed system using three different optimization algorithms. All three optimization algorithms aim to strike a balance between conflicting objectives, such as increasing power production, reducing fuel consumption, and minimizing environmental impacts. The results indicate that these algorithms have somewhat succeeded in achieving this balance. Overall, the findings suggest that the NSGA-III algorithm provides greater improvements compared to the other optimization algorithms in terms of system performance parameters. The MOGOA method has created a more balanced improvement in the simultaneous production system, while the MOMVO, despite optimizing the system, has shown less improvement in performance parameters compared to the other two algorithms.

Optimization using the NSGA-III method has increased freshwater production and energy efficiency by 30.77 % and 54.04 %, respectively, showing greater improvements compared to the other algorithms under consideration. Additionally, this method has improved exergy destruction, return on investment, and environmental impact rate by 19.01 %, 38.82 %, and 6.39 %, respectively, demonstrating its excellent performance for energy systems.

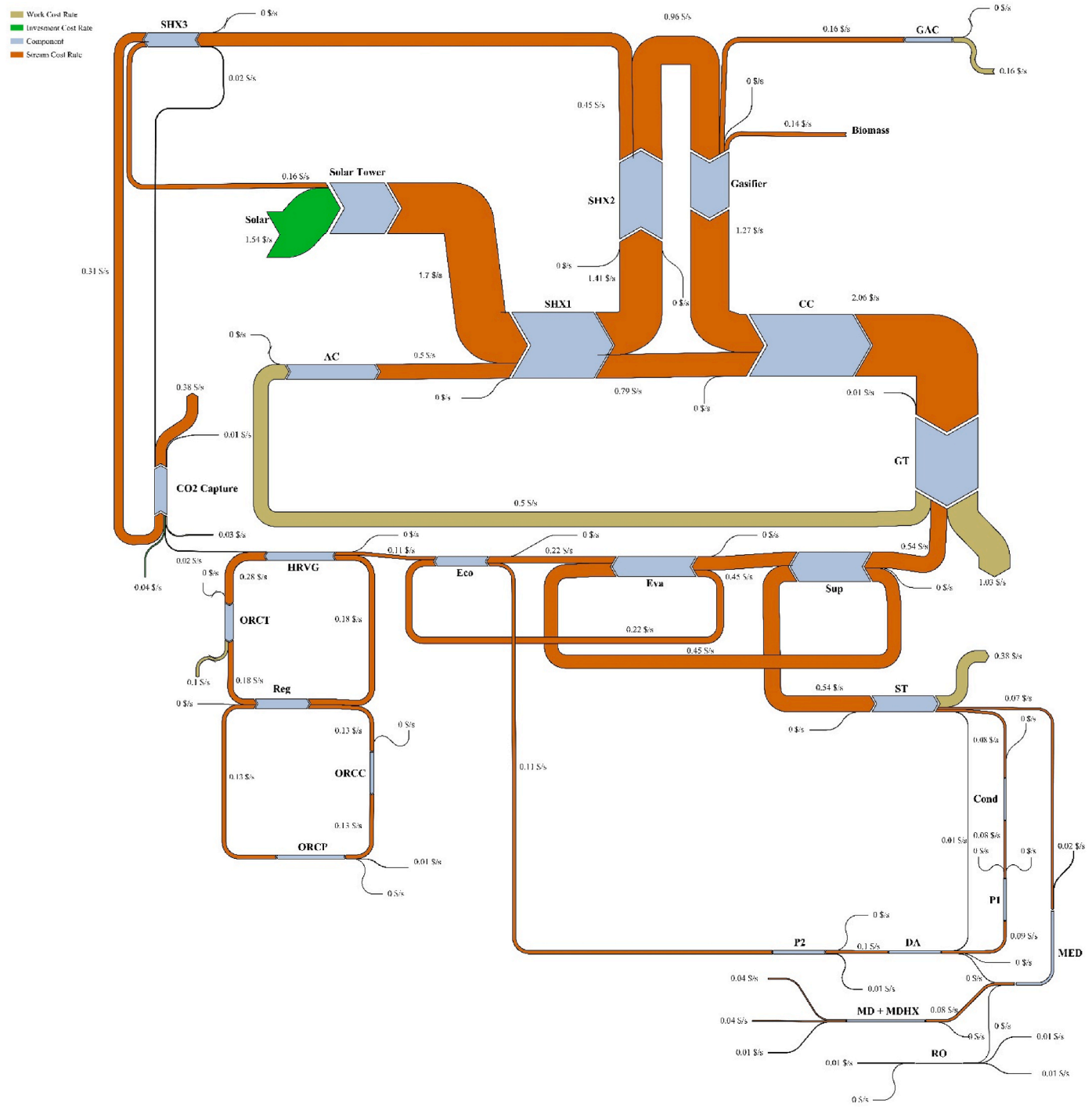

Fig. 18. Optimal exergoeconomic Sankey diagram of the proposed system.

Fig. 15 illustrates the 2D and 3D Pareto fronts obtained from the multi-objective optimization process using NSGA-III, which was identified as the most effective algorithm among the tested methods. The Pareto front clearly demonstrates the trade-offs between cogeneration efficiency, payback period, and environmental impact rate. By examining the distribution of solutions, decision-makers can select a suitable configuration based on their priorities.

Figs. 16–19 illustrate the system's performance in its optimized state. Fig. 16 shows the block flow diagram of energy results, providing a clear overview of energy distribution and efficiency. Figs. 17–19 depict Sankey diagrams for exergy, exergoeconomic, and exergoenvironmental analyses, respectively. These diagrams visually emphasize the flow distribution and losses, underscoring the system's sustainability and economic viability.

The exergy analysis (Fig. 17) reveals opportunities for improving energy utilization, while the exergoeconomic and exergoenvironmental diagrams (Figs. 18 and 19) highlight cost-effective and environmentally friendly pathways. These findings align with SDG 7 (Affordable and Clean Energy) and SDG 12 (Responsible Consumption and Production), supporting global efforts toward sustainable energy systems.

Overall, the proposed hybrid solar-biomass cogeneration system offers a promising solution for sustainable power and water supply in remote regions such as the Canary Islands. The results align with several United Nations Sustainable Development Goals (SDGs), including SDG 6

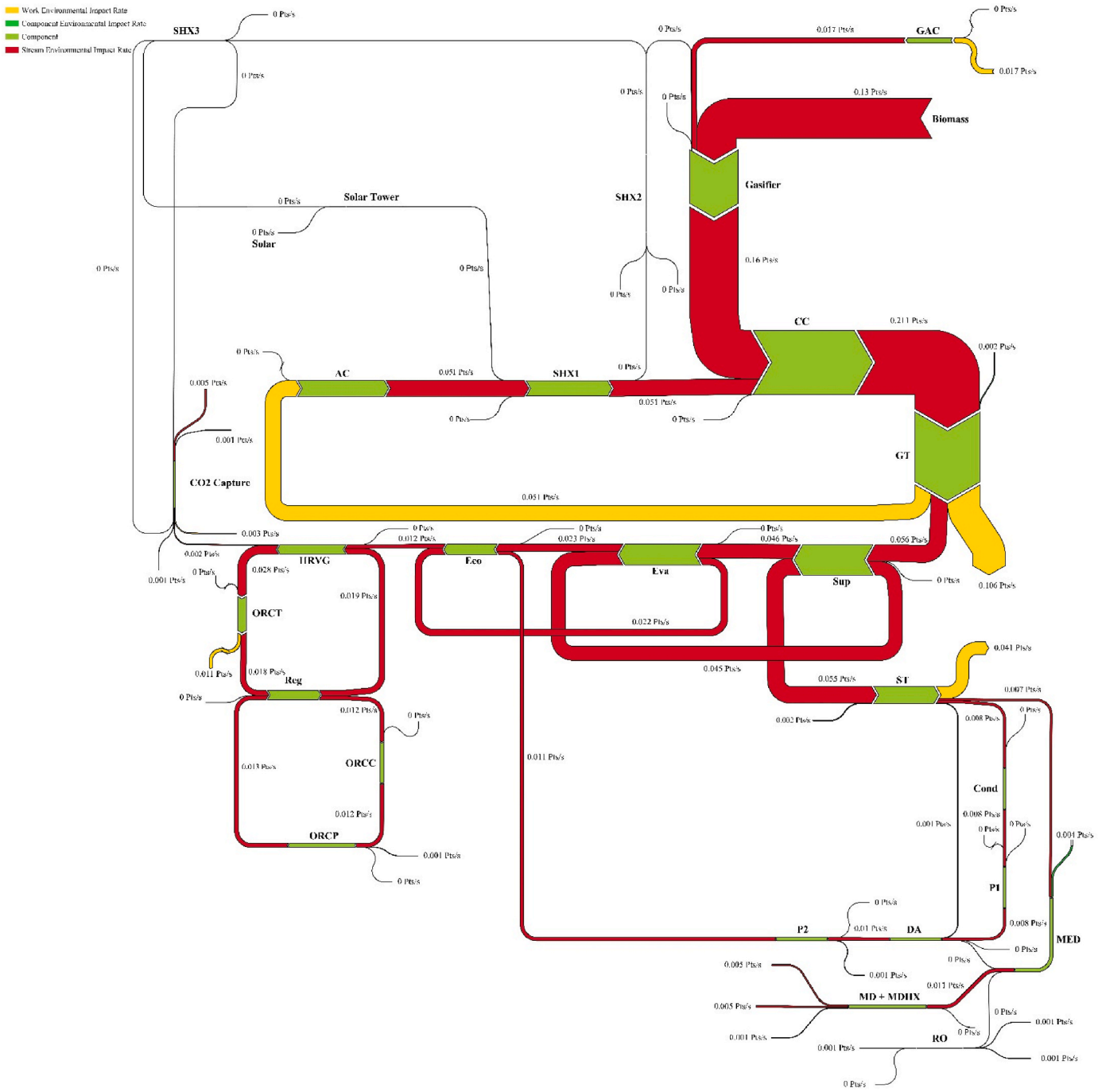

Fig. 19. Optimal exergoenvironmental Sankey diagram of the proposed system.

(Clean Water and Sanitation), SDG 7 (Affordable and Clean Energy), SDG 12 (Responsible Consumption and Production), and SDG 13 (Climate Action). The integration of renewable energy sources, waste heat recovery, and carbon mitigation strategies confirms the system's technical, economic, and environmental viability. Future research could explore further system improvements through advanced control techniques, seasonal storage integration, and real-world pilot testing.

6. Conclusions

The present work presents an innovative solar-biomass cogeneration system for power and freshwater production in Canary Islands, Spain. The proposed system combines the Brayton cycle, steam Rankine cycle, and organic Rankine cycle for power generation, alongside multi-effect distillation, reverse osmosis, and membrane distillation for freshwater production. A CO_2 capture unit is integrated to reduce environmental emissions. The solar field supplies the required heat through the solar tower, while biomass energy is provided by the air-steam gasification unit using locally sourced Canary Pine Needles. Machine learning techniques are employed to analyze the subsystems. The system's feasibility is assessed through technical-economic analysis and life cycle assessment, with dynamic modeling based on the climatic conditions of Las Palmas. Lastly, sensitivity analysis and multi-objective optimization were performed using three algorithms—NSGA-III, MOMVO, and MOGOA—to optimize the system's performance. The analysis of the annual average performance of the proposed system revealed that the energy and exergy efficiencies are 31.64 % and 14.35 %, respectively. The levelized cost and environmental impacts of electricity in the

current system are 0.19 $/kWh and 1.24 mPts/kWh. Additional key results from the analysis of the proposed system include.

- The exergy destruction in the solar field is higher than in other parts of the system.
- The gas turbine (GT) exhibits the highest exergy efficiency in the proposed system.
- The desalination sector has higher environmental impacts compared to the rest of the system.
- The payback period is 3.22 years with an interest rate of 10 %.
- The cost and environmental impact of freshwater production are 2.53 $/m^3 and 540.08 mPts/m^3, respectively.
- Energy, exergy efficiency, and cost equivalent to electricity are lower during the summer season.
- NSGA-III has shown better performance in optimizing the system's functional parameters compared to other optimization methods.
- The NSGA-III optimization of the proposed system led to a 54.04 % improvement in cogeneration efficiency, a 38.82 % reduction in payback period, and a 6.39 % decrease in environmental impact rate.

In future research, it is essential to explore alternative biomass fuels, particularly those that are locally available and sustainable, to ensure their long-term suitability for the proposed system. Additionally, a thorough examination of the system's layout, along with the creation of P&ID (Piping and Instrumentation Diagrams), PFD (Process Flow Diagrams), and piping maps, will be critical before the implementation phase. These steps will allow for the refinement of the design and ensure that the system operates efficiently and is feasible for real-world application.

CRediT authorship contribution statement

Seyed Alireza Mousavi Rabeti: Writing – original draft, Visualization, Validation, Software, Methodology, Investigation, Formal analysis. **Mohammad Hasan Khoshgoftar Manesh:** Writing – review & editing, Validation, Software, Methodology, Investigation, Conceptualization. **Ana María Blanco-Marigorta:** Writing – review & editing, Resources, Methodology, Investigation. **B. Del Río-Gamero:** Writing – review & editing, Investigation, Formal analysis, Data curation.

Declaration of competing interest

The authors declare that they have no known competing financial interests or personal relationships that could have appeared to influence the work reported in this paper.

Acknowledgment

This research has been co-funded by ERDF funds, INTERREG MAC 2014–2020 programmee, within the E5DES project (MAC2/1.1a/309). No funding sources had any influence on study design, collection, analysis, or interpretation of data, manuscript preparation, or the decision to submit for publication.

Appendix

Table A.1
Equations are required to calculate the cost and weight of the equipment used [83].

Component	Cost equations ($)	Weight equations (ton)
Compressors	$PEC = 71.1 \times \frac{\dot{m}}{0.92 - \eta_C} \times r_p \times \ln(r_p)$	$\rho = \frac{P_o}{R \times T_o}$. $A = \frac{\dot{m}}{\rho \times vel}$. $D = \sqrt{\frac{4}{\pi \times A}}$. $Weight = \frac{P_o \times D \times FS}{2 \times \sigma}$
Combustion chamber	$PEC = 46.08 \times \frac{\dot{m}_a}{0.995 - \frac{P_o}{P_i}} \times (1 + \exp(0.018 \times T_o - 26.4))$	$\rho = \frac{P_o}{R_{fg} \times T_o}$. $A = \frac{\dot{m}_{fg}}{\rho \times vel}$. $D = \sqrt{\frac{4}{\pi \times A}}$. $Weight = \frac{P_o \times D \times FS}{2 \times \sigma}$
Condensers	$PEC = 1773 \dot{m}_{Cooled\ Fluid}$	$Weight = 0.073\left(\frac{\dot{Q}_{Cond}}{1000}\right)^{0.99}$
Deaerator	$PEC = 145315 \times (\dot{m}_{DA})^{0.7}$ [84]	$Weight = 2.49 \times (\dot{m}_{DA})^{0.7}$
Gas turbine	$PEC = 479.34 \times \frac{\dot{m}_{fg}}{0.93 - \eta_{GT}} \times \ln(\frac{P_i}{P_o}) \times (1 + \exp(0.036 \times T_i - 54.4))$	$\rho = \frac{P_o}{R_{fg} \times T_o}$. $A = \frac{\dot{m}_{fg}}{\rho \times vel}$. $D = \sqrt{\frac{4}{\pi \times A}}$. $Weight = \frac{P_o \times D \times FS}{2 \times \sigma}$
Gasifier	$PEC = 1600 \times (\dot{m}_{Bio} \times 3600)^{0.67}$ [85]	$\rho = \frac{P_o}{R_{sg} \times T_o}$. $A = \frac{\dot{m}_{fg}}{\rho \times vel}$. $D = \sqrt{\frac{4}{\pi \times A}}$. $Weight = \frac{P_o \times D \times FS}{2 \times \sigma}$
Heat exchanger	$PEC = 235 \times \dot{Q}_{Hx}^{0.75}$ [86]	$Weight = 2.14 \times \left(\frac{\dot{Q}_{Hx}}{1000}\right)^{0.7}$
HRSG	$PEC = \left[\left(\frac{\dot{Q}_{ECO}}{\Delta T_{ECO}}\right)^{0.8} + \left(\frac{\dot{Q}_{EVA}}{\Delta T_{EVA}}\right)^{0.8} + \left(\frac{\dot{Q}_{SH}}{\Delta T_{SH}}\right)^{0.8}\right] + 21276\dot{m}_w + 1184.4\dot{m}_{fg}^{1.2}$	$Weight_{SH} = 8.424 \times \left(\frac{\dot{Q}_{SH}}{1000}\right)^{0.87}$ $Weight_{EVA} = 13.91 \times \left(\frac{\dot{Q}_{EVA}}{1000}\right)^{0.68}$ $Weight_{ECO} = 2.989 \times \left(\frac{\dot{Q}_{ECO}}{1000}\right)^{0.98}$
MED	$PEC = 12000\left(\frac{A_{MED}}{100}\right)^{0.6}$	Environmental Impact of MED calculated directly independent of its weight
ORCP	$PEC = 2100\left(\frac{\dot{W}_{ORCP}}{10}\right)^{0.26} \times \left(\frac{1 - \eta_{ORCP}}{\eta_{ORCP}}\right)^{0.5}$	$Weight = 0.0061 \times \dot{W}_{ORCP}^{0.95}$
OPCT	$PEC = \frac{497.34\dot{m}_{ORC}}{0.92 - \eta_{ORCT}} \ln\left(\frac{P_1}{p_2}\right)(1 + \exp(0.036T_1 - 54.4))$ [87]	$Weight = 4.9 \times \dot{W}_{ORCT}^{0.7}$
Solar tower	$PEC = (83764759.98) + (0.00819 \times \dot{Q}_{REC}^{\ 2}) - \left(85.75 \times \left(\frac{\Delta T}{2}\right)^2\right)$ [88]	$Weight = (0.02840879\ \dot{Q}_{REC}) - 0.027175$ [88]
Pumps	$PEC = 2100\left(\frac{\dot{W}_P}{10}\right)^{0.26} \times \left(\frac{1 - \eta_P}{\eta_P}\right)^{0.5}$	$Weight = 0.0061 \times \dot{W}_P^{0.95}$
RO	$PEC = PEC_{membrane} + PEC_{pretreat} + PEC_{RO-P} + PEC_{RO-valve}$ [89] $PEC_{membrane} = N_{memb} \times PEC_{One-membrane}$	Environmental Impact of RO calculated directly independent of its weight

(*continued on next page*)

Table A.1 (*continued*)

Component	Cost equations ($)	Weight equations (ton)
	$PEC_{One-membrane} = 7846$	
	$PEC_{pretreat} = 996 \times 1.399 \times \left(\frac{\dot{m}_{RO-Feed}}{\rho} \times 24 \times 3600\right)^{0.8}$	
	$PEC_{RO-P} = 393000 \times 1.399 + 701.19 \times 14.5 \times P_{RO-Feed}$	
	$PEC_{RO-valve} = 8.07 \times 0.989 \times \dot{m} \times \left(\frac{T_i}{P_i}\right)^{0.05} \times P_o^{-0.75}$ [90,91]	
ST	$PEC = 2210 \times \dot{W}_{ST}^{0.7}$	$Weight = 4.9 \times \dot{W}_{ST}^{0.73}$
MD	$PEC = PEC_{membrane} + PEC_{pretreat} + PEC_{Storage} + PEC_{Size\ development}$ [92]	Environmental Impact of MD calculated directly independent of its weight
	$PEC_{membrane} = \frac{m_F}{J_w} \times 60$	
	$PEC_{pretreat} = 79.25 \times m_D PEC_{Storage} = 42.27 \times m_D PEC_{Size\ development} = 26.42 \times m_D$	
CO_2 capture	$PEC = 0.074\ \$/kg\ CO_2$ [93]	$Weight = 10 \times \left(37.27\dot{m}_{fg} + 0.1312\dot{m}_{fg}^2\right)$ [93]

Table A.2
4E results of all streams for the proposed cogeneration system on June 21 (12 h of noon.)

Stream No.	Fluid	$\dot{m}_i(kg/s)$	$T_i(^\circ C)$	$P_i(bar)$	$\dot{E}x_i(MW)$	$\dot{C}_i(\$/s)$	$\dot{B}_i(mPts/s)$
1	*Air*	20.25	26.25	1.03	0.00	0.00	0.00
2	*Air*	20.25	429.15	15.68	7.88	0.85	60.21
3	*Air*	20.25	600.00	15.37	10.19	1.52	60.34
4	*Flue gas*	32.96	1149	14.91	33.02	3.19	223.40
5	*Flue gas*	32.96	541.13	1.11	8.62	0.83	58.31
6	*Biomass*	2.42	26.25	1.03	72.91	0.15	0.01
7	*Water*	3.06	20.00	1.03	0.00	0.00	0.00
8	*Water*	3.06	20.07	10.20	0.00	0.00	0.03
9	*Water*	3.06	197.87	10.00	2.53	1.28	0.28
10	*Air*	7.23	26.25	1.025	0.00	0.00	0.00
11	*Air*	7.23	342.54	10.00	2.17	0.24	16.72
12	*Syngas*	12.71	796.23	10.00	49.36	1.67	162.83
13	*Flue gas*	32.96	482.34	1.09	7.16	0.69	48.44
14	*Flue gas*	32.96	324.80	1.07	3.73	0.36	25.21
15	*Flue gas*	32.96	233.44	1.05	2.06	0.20	13.95
16	*Water*	4.37	450.00	90.00	5.78	0.80	55.78
17	*Water*	0.27	124.69	2.30	0.15	0.02	1.47
18	*Water*	1.58	99.88	1.01	0.70	0.10	6.72
19	*Water*	2.53	81.38	0.5	0.86	0.12	8.29
20	*Water*	1.58	99.90	2.30	0.05	0.01	0.50
21	*Water*	2.53	81.32	0.5	0.05	0.12	8.29
22	*Water*	2.53	81.38	2.30	0.05	0.12	8.30
23	*Water*	4.10	92.80	2.30	0.11	0.13	8.80
24	*Water*	4.37	124.69	2.30	0.25	0.15	10.27
25	*Water*	4.37	128.43	95.62	0.30	0.16	11.39
26	*Water*	4.37	301.26	93.71	1.66	0.32	22.67
27	*Water*	4.37	304.79	91.83	4.59	0.66	45.89
28	*Water*	124.81	20.00	1.03	0.03	0.00	0.00
29	*Water*	124.81	30.00	1.03	0.01	0.00	0.00
30	*Flue gas*	32.96	100.00	1.03	0.39	0.04	2.62
31	*Isobutane*	15.41	150	14.00	2.18	0.49	34.17
32	*Isobutane*	15.41	121.99	5.10	1.39	0.31	21.70
33	*Isobutane*	15.41	37.71	5.00	0.97	0.22	15.15
34	*Isobutane*	15.41	37.71	5.00	0.80	0.22	15.15
35	*Isobutane*	15.41	39.16	14.58	0.83	0.23	16.30
36	*Isobutane*	15.41	82.99	14.28	1.20	0.33	22.85
37	*Water*	107.74	20.00	1.03	0.03	0.00	0.00
38	*Water*	107.74	30.00	1.03	0.01	0.00	0.00
39	*Clean gas*	32.34	35.00	1.03	0.09	0.01	0.61
40	*Carbon dioxide*	0.51	45.00	150.00	0.12	0.64	5.91
41	*Water*	1.70	151.83	5.00	1.21	1.63	0.11
42	*Water*	1.70	100.30	1.03	0.06	0.55	0.01
43	*Water*	54.95	26.25	3.00	0.00	0.00	0.00
44	*Water*	54.95	36.25	3.00	0.02	0.00	0.00
45	*Sodium liquid*	29.74	900.00	95	17.82	3.90	0.80
46	*Sodium liquid*	29.74	800.00	93.10	14.77	3.23	0.64
47	*Sodium liquid*	29.74	577.84	91.24	8.92	1.95	0.39
48	*Sodium liquid*	29.74	20.00	89.41	6.50	1.42	0.28
49	*Sodium liquid*	29.74	472.58	96.38	6.51	1.42	0.49
50	*Seawater*	35.70	20.00	1.11	0.01	0.00	0.00
51	*Seawater*	30.70	35.00	1.11	0.01	0.00	0.00
52	*Seawater*	29.17	35.00	1.11	0.01	0.00	0.00
53	*Freshwater*	17.83	35.00	1.03	0.01	0.01	0.97
54	*Brine*	12.87	35.56	1.03	0.04	0.00	0.00

(*continued on next page*)

Table A.2 (*continued*)

Stream No.	Fluid	$\dot{m}_i(kg/s)$	$T_i(^\circ C)$	$P_i(bar)$	$\dot{E}x_i(MW)$	$\dot{C}_i(\$/s)$	$\dot{B}_i(mPts/s)$
55	*Seawater*	1.54	35.00	1.11	0.00	0.00	0.00
56	*Freshwater*	3.79	86.68	4.00	0.09	0.15	11.22
57	*Brine*	1.21	60.00	1.03	0.01	0.00	0.00
58	*Freshwater*	3.79	68.61	3.92	0.04	0.08	5.77
59	*Seawater*	1.54	81.68	1.03	0.03	0.07	5.45
60	*Brine*	2.76	72.21	1.03	0.04	0.07	5.45
61	*Brine*	2.75	66.46	1.03	0.03	0.06	4.21
62	*Seawater*	4.14	20.00	1.03	0.00	0.00	0.00
63	*Seawater*	4.14	33.00	1.03	0.00	0.00	0.00
64	*Seawater*	35.75	20.00	1.03	0.01	0.00	0.00
MD Distillate	*Freshwater*	0.01	47.92	1.03	0.00	0.02	1.25

References

[1] N. Melián-Martel, B. del Río-Gamero, J. Schallenberg-Rodriguez, Water cycle driven only by wind energy surplus: towards 100% renewable energy islands, Desalination 515 (2021) 115216.

[2] E. Rosales-Asensio, et al., Stress mitigation of conventional water resources in water-scarce areas through the use of renewable energy powered desalination plants: an application to the Canary Islands, Energy Rep. 6 (2020) 124–135.

[3] K. Guerra, et al., Facing the high share of variable renewable energy in the power system: flexibility and stability requirements, Appl. Energy 310 (2022) 118561.

[4] S.M. Rabeti, M.K. Manesh, M. Amidpour, Techno-economic and environmental assessment of a novel polygeneration system based on integration of biomass air-steam gasification and solar parabolic trough collector, Sustain. Energy Technol. Assessments 56 (2023) 103030.

[5] X. Sun, et al., Hubs and clusters approach to unlock the development of carbon capture and storage–case study in Spain, Appl. Energy 300 (2021) 117418.

[6] M.H.K. Manesh, S. Davadgaran, S.A.M. Rabeti, Novel solar-biomass polygeneration system based on integration of ICE-ORC-MDC-HDH-RO and tomato greenhouse to produce power, freshwater, and biological wastewater treatment, Energy Convers. Manag. 308 (2024) 118349.

[7] S.A.M. Rabeti, M.H.K. Manesh, M. Amidpour, An innovative optimal 4E solar-biomass waste polygeneration system for power, methanol, and freshwater production, J. Clean. Prod. 412 (2023) 137267.

[8] O. Siddiqui, I. Dincer, Design and assessment of a new solar-based biomass gasification system for hydrogen, cooling, power and fresh water production utilizing rice husk biomass, Energy Convers. Manag. 236 (2021) 114001.

[9] M.A. Khadimallah, et al., Simultaneous power, fresh water and fuel generation using a novel hybrid system based on biomass and solar thermal energy, Int. J. Hydrogen Energy 70 (2024) 414–428.

[10] A. Bozgeyik, L. Altay, A. Hepbasli, Energetic, exergetic, exergoeconomic, environmental and sustainability analyses of a solar, geothermal and biomass based novel multi-generation system for production of power, hydrogen, heating, cooling and fresh water, Process Saf. Environ. Prot. 177 (2023) 400–415.

[11] N. Khani, M.K. Manesh, V. Onishi, 6E analyses of a new solar energy-driven polygeneration system integrating CO2 capture, organic rankine cycle, and humidification-dehumidification desalination, J. Clean. Prod. (2022) 134478.

[12] H. Noorbakhsh, M.H.K. Manesh, M. Amidpour, Evaluation of an innovative polygeneration system based on integration of gasification process with a thermo electric generator-solid oxide fuel cell-adsorption desalination system-thermal photovoltaic collector, Energy (2023) 128672.

[13] Y. Zhu, et al., Thermodynamic analysis and economic assessment of biomass-fired organic rankine cycle combined heat and power system integrated with CO2 capture, Energy Convers. Manag. 204 (2020) 112310.

[14] M.H.K. Manesh, S. Davadgaran, S.A.M. Rabeti, New procedure for designing an innovative biomass-solar-wind polygeneration system for sustainable production of power, freshwater, and ammonia using 6E analyses, carbon footprint, water footprint, and multi-objective optimization, Renew. Energy (2024) 120802.

[15] U. Ahmed, Techno-economic analysis of dual methanol and hydrogen production using energy mix systems with CO2 capture, Energy Convers. Manag. 228 (2021) 113663.

[16] S.A.M. Rabeti, et al., Development of a new strategy for selecting solar desalination plants based on techno-economic, environmental, and climatic issues: the case study of Iran, Sustain. Energy Technol. Assessments 73 (2025) 104122.

[17] K.S. Chauhan, R. Beniwal, H. Tyagi, Thermodynamic analysis of a hybrid novel solar powered humidification-dehumidification coupled with direct contact membrane distillation system, Energy Convers. Manag. 300 (2024) 117930.

[18] A.A. Alazab, N.A. Qasem, H. Baaqeel, Performance evaluation of a novel integrated adsorption desalination system with direct contact membrane distillation plant, Desalination 552 (2023) 116441.

[19] M. Morid, M.H.K. Manesh, 6E evaluation of an innovative polygeneration system consisting of gas turbine cycle with CO2 capture, ejector refrigeration cycle, steam rankine cycle, solar tower and MEDAD unit, Therm. Sci. Eng. Prog. (2023) 102234.

[20] M.H.K. Manesh, et al., Optimal 4E evaluation of an innovative solar-wind cogeneration system for sustainable power and fresh water production based on integration of microbial desalination cell, humidification-dehumidification, and reverse osmosis desalination, Energy (2024) 131256.

[21] M. Nourpour, M.H.K. Manesh, Availability and 6E assessment and optimal design of a novel cogeneration system based on integrated Turbo compressor station-SOFC-solar-geothermal-steam and organic rankine cycles with machine learning, Renew. Energy 215 (2023) 118908.

[22] S.A.M. Rabeti, M.H.K. Manesh, M. Amidpour, Optimal 4E design and innovative R-Curve approach for a gas-solar-biological waste polygeneration system for power, freshwater, and methanol production, Process Saf. Environ. Prot. (2024).

[23] H. Vazini Modabber, M.H. Khoshgoftar Manesh, Optimal exergetic, exergoeconomic and exergoenvironmental design of polygeneration system based on gas turbine-absorption chiller-solar parabolic trough collector units integrated with multi-effect desalination-thermal vapor compressor- reverse osmosis desalination systems, Renew. Energy 165 (2021) 533–552.

[24] M.J. Mehrabian, M.H.K. Manesh, D.H. Jeong, 4E and risk assessment of a novel integrated biomass driven polygeneration system based on integrated sCO2-ORC-AD-SOFC-SOEC-PEMFC-PEMEC, Sustain. Energy Technol. Assessments 58 (2023) 103317.

[25] H.V. Modabber, S.A.M. Rabeti, New optimal scheme for the poly-generation system, integrated with ORC and hydrogen production units, using technical, emergy, and thermo-risk analyses-case study for qeshm power and water co-generation plant, Therm. Sci. Eng. Prog. 36 (2022) 101506.

[26] M. Ebadollahi, et al., Proposal and multi-criteria optimization of two new combined heating and power systems for the Sabalan geothermal source, J. Clean. Prod. 229 (2019) 1065–1081.

[27] M.H. Khoshgoftar Manesh, V.C. Onishi, Energy, exergy, and thermo-economic analysis of renewable energy-driven polygeneration systems for sustainable desalination, Processes 9 (2) (2021) 210.

[28] L.F. Prieto, G.R. Rodríguez, J.S. Rodríguez, Wave energy to power a desalination plant in the north of gran canaria island: wave resource, socioeconomic and environmental assessment, J. Environ. Manag. 231 (2019) 546–551.

[29] G. Barone, et al., Increasing renewable energy penetration and energy Independence of island communities: a novel dynamic simulation approach for energy, economic, and environmental analysis, and optimization, J. Clean. Prod. 311 (2021) 127558.

[30] S.F. Moosavian, Y. Noorollahi, M. Shoaei, Renewable energy resources utilization planning for sustainable energy system development on a stand-alone island, J. Clean. Prod. (2024) 140892.

[31] R.-E. Dong, et al., A heat recovery-based ecofriendly solar thermal-driven electricity/hydrogen/freshwater multigeneration scheme using LNG regasification: energy, exergy, economic, and environmental (4E) analysis, Case Stud. Therm. Eng. 53 (2024) 103853.

[32] N. Mir, Y. Bicer, Integration of electrodialysis with renewable energy sources for sustainable freshwater production: a review, J. Environ. Manag. 289 (2021) 112496.

[33] Mousazade, M.R., et al., Mathematical modeling of waste engine oil gasification for synthesis gas production; operating parameters and simulation. Int. J. Therm.: p. 1-13.

[34] Á. Rivero-Falcón, B. Peñate Suárez, N. Melián-Martel, SWRO brine characterisation and critical analysis of its industrial valorisation: a case study in the Canary Islands (spain), Water 15 (8) (2023) 1600.

[35] K. Nakoa, A. Date, A. Akbarzadeh, A research on water desalination using membrane distillation, Desalination Water Treat. 56 (10) (2015) 2618–2630.

[36] L. Díaz, et al., Assessment of the energy potential of agricultural and forestry biomass sources from the Canary Islands, RE&PQJ 20 (4) (2022).

[37] N. Khani, M.H.K. Manesh, V.C. Onishi, Optimal 6E design of an integrated solar energy-driven polygeneration and CO2 capture system: a machine learning approach, Therm. Sci. Eng. Prog. 38 (2023) 101669.

[38] M. Amidpour, M.H.K. Mansh, Cogeneration and Polygeneration Systems, Academic Press, 2020.

[39] Z. Ghaffarpour, et al., Thermoeconomic assessment of a novel integrated biomass based power generation system including gas turbine cycle, solid oxide fuel cell and rankine cycle, Energy Convers. Manag. 161 (2018) 1–12.

[40] M.H.K. Manesh, S. Davadgaran, S.A.M. Rabeti, Gasification potential of municipal solid waste in Iran: application of life cycle assessment, risk analysis, and machine learning, J. Clean. Prod. 434 (2024) 140177.

[41] M.H. Khoshgoftar Manesh, N. Abbasi, M.J. Mehrabian, Optimal design of a novel hybrid solar tower-gas turbine combined cycle with proton exchange membrane

polygeneration system: application of machine learning, Environ. Prog. Sustain. Energy 42 (3) (2023) e14029.
[42] M. Fallahzadeh, M.H.K. Manesh, B. Ghorbani, New procedure for an optimal design of an integrated solar tower power plant with supercritical carbon dioxide and organic rankine cycle and MED-RO desalination based on 6E analysis, Sustain. Energy Technol. Assessments 60 (2023) 103522.
[43] S. Hou, et al., Optimization of the combined supercritical CO2 cycle and organic rankine cycle using zeotropic mixtures for gas turbine waste heat recovery, Energy Convers. Manag. 160 (2018) 313–325.
[44] H. Vazini Modabber, M.H. Khoshgoftar Manesh, 4E analysis of power and water cogeneration plant based on integrated MED-TVC and RO desalination units, Int. J. Therm. 23 (2) (2020) 107–126.
[45] E. Ali, et al., Integration of multi effect evaporation and membrane distillation desalination processes for enhanced performance and recovery ratios, Desalination 493 (2020) 114619.
[46] S. Channiwala, P. Parikh, A unified correlation for estimating HHV of solid, liquid and gaseous fuels, Fuel 81 (8) (2002) 1051–1063.
[47] T.J. Kotas, The Exergy Method of Thermal Plant Analysis, Paragon Publishing, 2012.
[48] K.J. Ptasinski, M.J. Prins, A. Pierik, Exergetic evaluation of biomass gasification, Energy 32 (4) (2007) 568–574.
[49] J. Szargut, Exergy analysis of thermal processes, Journal of Power Technologies 84 (1996).
[50] M.H. Sharqawy, S.M. Zubair, Second law analysis of reverse osmosis desalination plants: an alternative design using pressure retarded osmosis, Energy 36 (11) (2011) 6617–6626.
[51] C. Tzivanidis, E. Bellos, K.A. Antonopoulos, Energetic and financial investigation of a stand-alone solar-thermal organic rankine cycle power plant, Energy Convers. Manag. 126 (2016) 421–433.
[52] H.I. Karali, H. Caliskan, Energy, exergy, sustainability, thermoeconomic, exergoeconomic, environmental and environmental-economic effects of novel boron-containing open cell geopolymer filter of a diesel engine on exhaust emissions, Energy 290 (2024) 130247.
[53] S.W. Sharshir, et al., Thermo-enviroeconomic assessment of a solar dryer of two various commodities, Energy 295 (2024) 130952.
[54] Z. Rahimimotlagh, A. Ahmadi, Energy, exergy, exergoeconomic and exergoenvironmental analysis and optimization of combined solar, SRC cycles with compressed air energy storage (CAES) and methane production system, Energy Convers. Manag. 317 (2024) 118855.
[55] M.K. Manesh, et al., Energy, exergy, exergoeconomic, and exergoenvironmental analysis of an innovative solar-geothermal-gas driven polygeneration system for combined power, hydrogen, hot water, and freshwater production, Sustain. Energy Technol. Assessments 51 (2022) 101861.
[56] H. Athari, et al., Gas turbine steam injection and combined power cycles using fog inlet cooling and biomass fuel: a thermodynamic assessment, Renew. Energy 92 (2016) 95–103.
[57] A. Bejan, G. Tsatsaronis, M.J. Moran, Thermal Design and Optimization, John Wiley & Sons, 1995.
[58] W. Ajeeb, R.C. Neto, P. Baptista, Life cycle assessment of green hydrogen production through electrolysis: a literature review, Sustain. Energy Technol. Assessments 69 (2024) 103923.
[59] M. Ji, J. Wang, Review and comparison of various hydrogen production methods based on costs and life cycle impact assessment indicators, Int. J. Hydrogen Energy 46 (78) (2021) 38612–38635.
[60] H. Blanco, et al., Life cycle assessment integration into energy system models: an application for power-to-methane in the EU, Appl. Energy 259 (2020) 114160.
[61] L. Meyer, et al., Exergoenvironmental analysis for evaluation of the environmental impact of energy conversion systems, Energy 34 (1) (2009) 75–89.
[62] E.J.C. Cavalcanti, Exergoeconomic and exergoenvironmental analyses of an integrated solar combined cycle system, Renew. Sustain. Energy Rev. 67 (2017) 507–519.
[63] G. Raluy, L. Serra, J. Uche, Life cycle assessment of MSF, MED and RO desalination technologies, Energy 31 (13) (2006) 2361–2372.
[64] Y. Liang, et al., Cradle-to-grave life cycle assessment of membrane distillation systems for sustainable seawater desalination, Energy Convers. Manag. 266 (2022) 115740.
[65] K. Deb, H. Jain, An evolutionary many-objective optimization algorithm using reference-point-based nondominated sorting approach, part I: solving problems with box constraints, IEEE Trans. Evol. Comput. 18 (4) (2013) 577–601.
[66] B. Zhou, et al., Multi-objective optimal operation of coastal hydro-electrical energy system with seawater reverse osmosis desalination based on constrained NSGA-III, Energy Convers. Manag. 207 (2020) 112533.
[67] S. Mirjalili, et al., Optimization of problems with multiple objectives using the multi-verse optimization algorithm, Knowl. Base Syst. 134 (2017) 50–71.
[68] F.M. Behbahani, B. Ahmadi, R. Caglar, Multi-objective multiverse optimization for optimal allocation of distributed energy resources: the optimal parallel processing schemes, Elec. Power Syst. Res. 231 (2024) 110298.
[69] S.Z. Mirjalili, et al., Grasshopper optimization algorithm for multi-objective optimization problems, Appl. Intell. 48 (2018) 805–820.
[70] P. Das, et al., Optimal reactive power dispatch and demand response in electricity market using multi-objective grasshopper optimization algorithm, Processes 12 (9) (2024) 2049.
[71] A. Al-Zahrani, et al., Thermodynamic analysis of a reverse osmosis desalination unit with energy recovery system, Procedia Eng. 33 (2012) 404–414.
[72] W. Zhou, L. Song, T.K. Guan, A numerical study on concentration polarization and system performance of spiral wound RO membrane modules, J. Membr. Sci. 271 (1–2) (2006) 38–46.
[73] T. Srinivas, A. Gupta, B. Reddy, Thermodynamic equilibrium model and exergy analysis of a biomass gasifier, J. Energy Resour. Technol. 131 (3) (2009).
[74] S. Jarungthammachote, A. Dutta, Thermodynamic equilibrium model and second law analysis of a downdraft waste gasifier, Energy 32 (9) (2007) 1660–1669.
[75] M.H.K. Manesh, et al., Feasibility study of green ammonia and electricity production via an innovative wind-solar-biomass polygeneration system, Appl. Energy 384 (2025) 125467.
[76] M. Morid, M.H.K. Manesh, An innovative optimal integrated solar-lignocellulosic biomass polygeneration system with biorefinery and solid oxide electrolyzer cell, Energy Convers. Manag. 327 (2025) 119557.
[77] H. Noorbakhsh, M.H.K. Manesh, M. Amidpour, Novel heavy fuel oil based IGCC polygeneration system based on integration with ejector cooling and heat recovery of the solid oxide fuel cell in adsorption desalination, Energy 312 (2024) 133488.
[78] Z.H. Tabriz, et al., Energy, exergy, exergoeconomic, and exergoenvironmental (4E) analysis of a new bio-waste driven multigeneration system for power, heating, hydrogen, and freshwater production: modeling and a case study in Izmir, Energy Convers. Manag. 288 (2023) 117130.
[79] F. Khalid, U. Akbulut, Exergoeconomic evaluation and optimization of a solar-powered polygeneration system producing freshwater, electricity, hydrogen, and cooling, Int. J. Hydrogen Energy (2024).
[80] M.M. Forootan, A. Ahmadi, Machine learning-based optimization and 4E analysis of renewable-based polygeneration system by integration of GT-SRC-ORC-SOFC-PEME-MED-RO using multi-objective grey wolf optimization algorithm and neural networks, Renew. Sustain. Energy Rev. 200 (2024) 114616.
[81] H. Hajabdollahi, A. Saleh, M. Shafiey Dehaj, A multi-generation system based on geothermal driven: energy, exergy, economic and exergoenvironmental (4E) analysis for combined power, freshwater, hydrogen, oxygen, and heating production, Environ. Dev. Sustain. 26 (10) (2024) 26415–26447.
[82] N. Hashemian, A. Noorpoor, M. Amidpour, A biomass assisted solar-based multi-generation plant with hydrogen and freshwater production: sustainability, advanced exergy and advanced exergo-economic assessments, in: Synergy Development in Renewables Assisted multi-carrier Systems, Springer, 2022, pp. 107–125.
[83] Z. Bai, et al., Thermodynamics evaluation of a solar-biomass power generation system integrated a two-stage gasifier, Energy Proc. 88 (2016) 368–374.
[84] M. Ameri, P. Ahmadi, A. Hamidi, Energy, exergy and exergoeconomic analysis of a steam power plant: a case study, Int. J. Energy Res. 33 (5) (2009) 499–512.
[85] A. Habibollahzade, E. Gholamian, A. Behzadi, Multi-objective optimization and comparative performance analysis of hybrid biomass-based solid oxide fuel cell/solid oxide electrolyzer cell/gas turbine using different gasification agents, Appl. Energy 233 (2019) 985–1002.
[86] N. Bonyadi, E. Johnson, D. Baker, Technoeconomic and exergy analysis of a solar geothermal hybrid electric power plant using a novel combined cycle, Energy Convers. Manag. 156 (2018) 542–554.
[87] H. Nami, S. Mahmoudi, A. Nemati, Exergy, economic and environmental impact assessment and optimization of a novel cogeneration system including a gas turbine, a supercritical CO2 and an organic rankine cycle (GT-HRSG/SCO2), Appl. Therm. Eng. 110 (2017) 1315–1330.
[88] N. Abbasi, M.H. Khoshgoftar Manesh, M. Yazdi, Dynamic analysis of a novel quadruple combined cycle based on integrated solar tower-gas turbine-supercritical CO2 and organic rankine cycles, J. Energy Resour. Technol. 144 (5) (2022).
[89] H.V. Modabber, M.K. Manesh, 4E dynamic analysis of a water-power cogeneration plant integrated with solar parabolic trough collector and absorption chiller, Therm. Sci. Eng. Prog. 21 (2021) 100785.
[90] Y.M. El-Sayed, The Thermoeconomics of Energy Conversions, Elsevier, 2013.
[91] C. Park, et al., Stochastic cost estimation approach for full-scale reverse osmosis desalination plants, J. Membr. Sci. 364 (1–2) (2010) 52–64.
[92] Z. Triki, Z. Fergani, M.N. Bouaziz, Exergoeconomic and exergoenvironmental evaluation of a solar-energy-integrated vacuum membrane distillation system for seawater desalination, Desal Water Treatment 225 (2021) 380–391.
[93] N. Khani, M.H.K. Manesh, V.C. Onishi, 6E analyses of a new solar energy-driven polygeneration system integrating CO2 capture, organic rankine cycle, and humidification-dehumidification desalination, J. Clean. Prod. 379 (2022) 134478.